Supporting Information:

Tuning of the Copper–Thioether Bond in Tetradentate $N_3S_{(thioether)}$ Ligands; O-O Bond Reductive Cleavage via a $[Cu^{II}_2(\mu\text{-}1,2\text{-peroxo})]^{2+}$ / $[Cu^{III}_2(\mu\text{-}oxo)_2]^{2+}$ Equilibrium

Sunghee Kim,[†] Jake W. Ginsbach,[‡] A. Imtiaz Billah,[†] Maxime A. Siegler,[†] Cathy D. Moore,[†] Edward I. Solomon,[‡]* and Kenneth D. Karlin[†]*

[†] Department of Chemistry, Johns Hopkins University, Baltimore, Maryland 21218

[‡] Department of Chemistry, Stanford University, Stanford, California 94305, United States

Contents:

1. X-ray crystallography

(a) [{(^{DMM}ESE)Cu^{I}}$_2$](B(C_6F_5)$_4$)$_2$ (**1$_2$**).

All reflection intensities were measured at 110(2) K using a KM4/Xcalibur (detector: Sapphire3) with enhance graphite-monochromated Mo *K*α radiation (λ = 0.71073 Å) under the program CrysAlisPro (Version 1.171.35.11 Oxford Diffraction Ltd., 2011). The program CrysAlisPro (Version 1.171.35.11, Oxford Diffraction Ltd., 2011) was used to refine the cell dimensions. Data reduction was done using the program CrysAlisPro (Version 1.171.35.11, Oxford Diffraction Ltd., 2011). The structure was solved with the program SHELXS-97 (Sheldrick, 2008) and was refined on F^2 with SHELXL-97 (Sheldrick, 2008). Analytical numeric absorption corrections based on a multifaceted crystal model were applied using CrysAlisPro (Version 1.171.35.11, Oxford Diffraction Ltd., 2011). The temperature of the data collection was controlled using the system Cryojet (manufactured by Oxford Instruments). The H atoms were placed at calculated positions using the instructions AFIX 23, AFIX 43 or AFIX 137 with isotropic displacement parameters having values 1.2 or 1.5 times *U*eq of the attached C atoms. The structure is ordered.

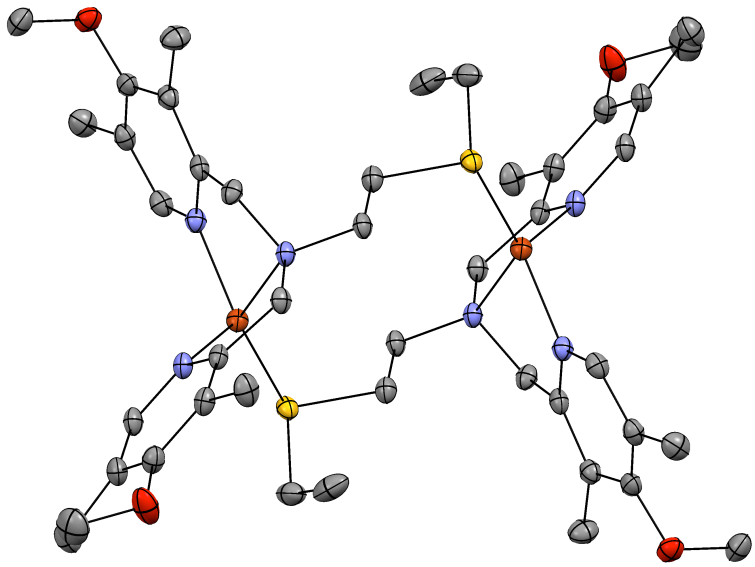

Figure S1. Displacement ellipsoid plot (50% probability level) of **1$_2$** at 110(2) K. The H atoms and the counterion are omitted for the sake of clarity. [{(^{DMM}ESE)Cu^{I}}$_2$](B(C_6F_5)$_4$)$_2$ (**1$_2$**). Fw = 2292.33, colorless parallelepiped, 0.38 × 0.30 × 0.08 mm^3, triclinic, *P*-1 (no. 2), a = 12.4411(3), b = 12.7513(3), c = 16.4894(4) Å, α = 98.1330(18), β = 102.8428(19), γ = 112.200(2)°, V = 2286.54(11) Å^3, Z = 1, D_x = 1.665 g cm^{-3}, μ = 0.649 mm^{-1}, T_{min}–T_{max}: 0.835–0.957. 27999 Reflections were measured up to a resolution of (sin $\theta/\lambda)_{max}$ = 0.62 Å^{-1}. 9224 Reflections were unique (R_{int} = 0.0253), of which 8008 were observed [$I > 2\sigma(I)$]. 674 Parameters were refined. $R1/wR2$ [$I > 2\sigma(I)$]: 0.0291/0.0741. $R1/wR2$ [all refl.]: 0.0358/0.0770. S = 1.043. Residual electron density found between −0.35 and 0.41 e Å^{-3}.

(b) [(^{DMM}ESE)Cu^{II}(ClO_4)](ClO_4) (**1a**)

All reflection intensities were measured at 150(2) K using a KM4/Xcalibur (detector: Sapphire3) with enhance graphite-monochromated Mo *K*α radiation (λ = 0.71073 Å) under the program CrysAlisPro (Version 1.171.35.11 Oxford Diffraction Ltd., 2011). The program CrysAlisPro (Version 1.171.35.11, Oxford Diffraction Ltd., 2011) was used to refine the cell dimensions. Data reduction was done using the program CrysAlisPro (Version 1.171.35.11, Oxford Diffraction Ltd., 2011). The structure was solved with the program SHELXS-97 (Sheldrick, 2008) and was refined on F^2 with SHELXL-97 (Sheldrick, 2008). Analytical numeric absorption corrections based on a multifaceted crystal model were applied using CrysAlisPro (Version 1.171.35.11, Oxford Diffraction Ltd., 2011). The temperature of the data collection was controlled using the system Cryojet (manufactured by Oxford Instruments). The H atoms were placed at calculated positions using the instructions AFIX 23, AFIX 43, AFIX 123 or AFIX 137 with isotropic displacement parameters having values 1.2 or 1.5 times *U*eq of the attached C atoms. The structure is ordered.

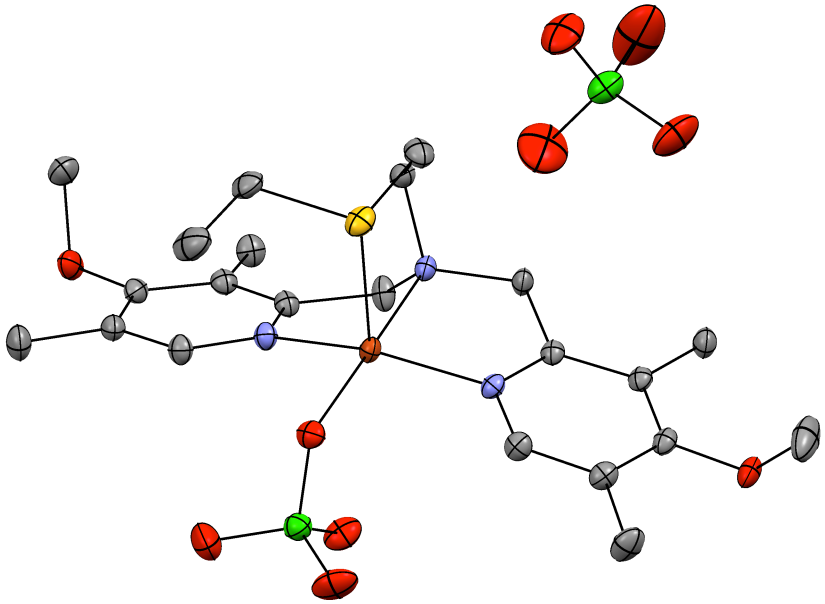

Figure S2. Displacement ellipsoid plot (50% probability level) of **1a** at 150(2) K. The H atoms are omitted for the sake of clarity. [(^{DMM}ESE)Cu^{II}(ClO_4)](ClO_4) (**1a**). Fw = 666.01, blue block, 0.59 × 0.47 × 0.15 mm^3, triclinic, *P*-1 (no. 2), a = 8.5031(2), b = 9.9656(3), c = 16.9854(5) Å, α = 93.826(3), β = 95.153(2), γ = 99.590(3)°, V = 1408.57(7) Å^3, Z = 2, D_x = 1.570 g cm^{-3}, μ = 1.097 mm^{-1}, T_{min}–T_{max}: 0.605–0.860. 19209 Reflections were measured up to a resolution of (sin $\theta/\lambda)_{max}$ = 0.65 Å^{-1}. 6467 Reflections were unique (R_{int} = 0.0255), of which 5847 were observed [$I > 2\sigma(I)$]. 358 Parameters were refined. $R1/wR2$ [$I > 2\sigma(I)$]: 0.0276/0.0720. $R1/wR2$ [all refl.]: 0.0310/0.0733. S = 1.058. Residual electron density found between -0.54 and 0.66 e Å^{-3}.

(c) [{(^{DMM}ESP)Cu^{I}}$_2$](B(C_6F_5)$_4$)$_2$ (**2$_2$**).

All reflection intensities were measured at 100(2) K using a SuperNova diffractometer (equipped with Atlas detector) with Cu *K*α radiation (mirror optics, λ = 1.54178 Å) under the program CrysAlisPro (Version 1.171.36.24 Agilent Technologies, 2012). The program CrysAlisPro (Version 1.171.36.24 Agilent Technologies, 2012) was used to refine the cell dimensions. Data reduction was done using the program CrysAlisPro (Version 1.171.36.24 Agilent Technologies, 2012). The structure was solved with the program SHELXS-97 (Sheldrick, 2008) and was refined on F^2 with SHELXL-97 (Sheldrick, 2008). Analytical numeric absorption corrections based on a multifaceted crystal model were applied using CrysAlisPro (Version 1.171.36.24 Agilent Technologies, 2012). The temperature of the data collection was controlled using the system Cryojet (manufactured by Oxford Instruments). The H atoms were placed at calculated positions using the instructions AFIX 23, AFIX 43, AFIX 123 or AFIX 137 with isotropic displacement parameters having values 1.2 or 1.5 times *U*eq of the attached C atoms. The structure is mostly ordered. The phenyl group C21→C26 is found to be disordered over two orientations, and the occupancy factor of the major component of the disorder refines to 0.665(16). The crystal lattice also contains some lattice pentane solvent molecules that are found to be disordered over two orientations, the occupancy factor of the major component of the disorder refines to 0.668(4).

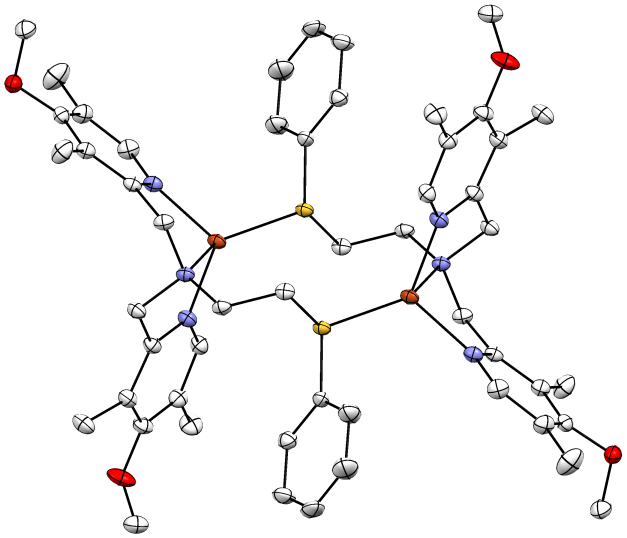

Figure S3. Displacement ellipsoid plot (50% probability level) of **2$_2$** at 100(2) K. The H atoms and the counterion are omitted for the sake of clarity. [{(^{DMM}ESP)Cu^{I}}$_2$](B(C_6F_5)$_4$)$_2$ (**2$_2$**). Fw = 2532.70, colorless needle, 0.49 × 0.10 × 0.08 mm^3, triclinic, *P*-1 (no. 2), *a* = 14.5520(5), *b* = 14.6344(5), *c* = 15.0327(6) Å, α = 67.739(3), *β* = 88.928(3), γ = 65.891(3)°, *V* = 2669.02(17) Å^3, *Z* = 1, D_x = 1.576 g cm^{-3}, *μ* = 1.989 mm^{-1}, T_{min}–T_{max}: 0.572–0.880. 31449 Reflections were measured up to a resolution of (sin *θ*/*λ*)$_{max}$ = 0.62 Å^{-1}. 10473 Reflections were unique (R_{int} = 0.0211), of which 9658 were observed [$I > 2\sigma(I)$]. 852 Parameters were refined using 317 restraints. *R*1/*wR*2 [$I > 2\sigma(I)$]: 0.0297/0.0763. *R*1/*wR*2 [all refl.]: 0.0324/0.0784. S = 1.030. Residual electron density found between −0.42 and 0.50 e Å^{-3}.

(d) [(^{DMM}ESP)Cu^{II}(H_2O)](ClO_4)$_2$ (**2a**).

All reflection intensities were measured at 240(2) K (All attempts to collect data below 200 K were unsuccessful because some significant crystal damage occurred while cooling the sample. The crystal damage might have resulted from a solid-solid phase transition through which molecular rearrangement might possibly be too large to sustain the room-temperature crystal morphology) using a SuperNova diffractometer (equipped with Atlas detector) with Cu *K*α radiation (λ = 1.54178 Å) under the program CrysAlisPro (Version 1.171.36.24 Agilent Technologies, 2012). The program CrysAlisPro (Version 1.171.36.24 Agilent Technologies, 2012) was used to refine the cell dimensions. Data reduction was done using the program CrysAlisPro (Version 1.171.36.24 Agilent Technologies, 2012). The structure was solved with the program SHELXS-2013 (Sheldrick, 2013) and was refined on F^2 with SHELXL-2013 (Sheldrick, 2013). Analytical numeric absorption corrections based on a multifaceted crystal model were applied using CrysAlisPro (Version 1.171.36.24 Agilent Technologies, 2012). The temperature of the data collection was controlled using the system Cryojet (manufactured by Oxford Instruments). The H atoms were placed at calculated positions (unless otherwise specified) using the instructions AFIX 23, AFIX 43 or AFIX 137 with isotropic displacement parameters having values 1.2 or 1.5 times *U*eq of the attached C atoms. The H atoms attached to the water molecule (O1) were found from Fourier difference maps, and their coordinates were refined freely (the O−H bond distances were restrained within acceptable ranges using the DFIX instructions). The structure is disordered. A part of the ligand N2→C26 and the two counterions are found to be disordered over two orientations. The occupancy factors of the major components of the disorder refine to 0.536(7), 0.823(5) and 0.646(7), respectively.

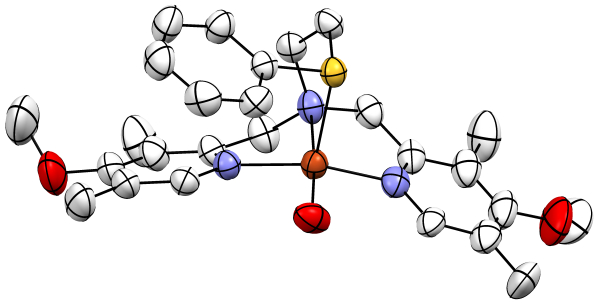

Figure S4. Displacement ellipsoid plot (50% probability level) of **2a** at 240(2) K. The H atoms and the counterions are omitted for the sake of clarity. [(^{DMM}ESP)Cu^{II}(H_2O)](ClO_4)$_2$ (2a): Fw = 732.07, blue thick lath, 0.46 × 0.30 × 0.16 mm^3, triclinic, *P*-1 (no. 2), a = 10.4003(5), b = 13.2758(7), c = 13.2819(7) Å, α = 66.056(5), β = 82.033(4), γ = 78.063(4)°, V = 1636.74(16) Å^3, Z = 2, D_x = 1.485 g cm^{-3}, μ = 3.561 mm^{-1}, T_{min}−T_{max}: 0.282−0.658. 19135 Reflections were measured up to a resolution of (sin $\theta/\lambda)_{max}$ = 0.62 Å^{-1}. 6428 Reflections were unique (R_{int} = 0.0169), of which 5884 were observed [$I > 2\sigma(I)$]. 598 Parameters were refined using 727 restraints. $R1/wR2$ [$I > 2\sigma(I)$]: 0.0378/0.1085. $R1/wR2$ [all refl.]: 0.0406/0.1114. S = 1.058. Residual electron density found between −0.39 and 0.61 e Å^{-3}.

(e) $[\{(^{DMM}ESDP)Cu^{I}\}_2](B(C_6F_5)_4)_2$ (**3₂**).

All reflection intensities were measured at 110(2) K using a SuperNova diffractometer (equipped with Atlas detector) with Cu *K*α radiation (λ = 1.54178 Å) under the program CrysAlisPro (Version 1.171.36.32 Agilent Technologies, 2013). The program CrysAlisPro (Version 1.171.36.32 Agilent Technologies, 2013) was used to refine the cell dimensions. Data reduction was done using the program CrysAlisPro (Version 1.171.36.32 Agilent Technologies, 2013). The structure was solved with the program SHELXS-2013 (Sheldrick, 2013) and was refined on F^2 with SHELXL-2013 (Sheldrick, 2013). Analytical numeric absorption corrections based on a multifaceted crystal model were applied using CrysAlisPro (Version 1.171.36.32 Agilent Technologies, 2013). The temperature of the data collection was controlled using the system Cryojet (manufactured by Oxford Instruments). The H atoms were placed at calculated positions using the instructions AFIX 23, AFIX 43 or AFIX 137 with isotropic displacement parameters having values 1.2 or 1.5 times *U*eq of the attached C atoms. The structure is mostly ordered. The part of the ligand N1→C15 is disordered over three orientations. The sum of the three occupancy factors was constrained to be equal to 1 (using the SUMP instruction), and these occupancy factors refine to 0.582(3), 0.312(3) and 0.106(2). The asymmetric unit contains one uncoordinated lattice THF molecule whose occupancy factor refines to 0.643(4), and this molecule was treated as ordered. Furthermore, some unresolved electron density – *i.e.*, most likely some small amount of (disordered) lattice solvent molecules is also found in the asymmetric unit. This contribution has been taken out in the final refinement (SQUEEZE details are provided in the CIF file).

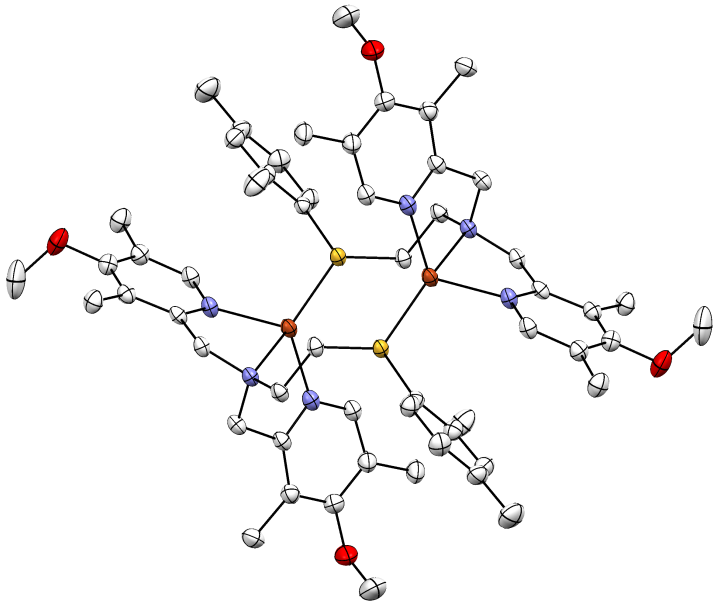

Figure S5. Displacement ellipsoid plot (50% probability level) of $\mathbf{3_2}$ at 110(2) K. The H atoms and the counterion are omitted for the sake of clarity. [{(^{DMM}ESDP)Cu^{I}}$_2$](B(C_6F_5)$_4$)$_2$ ($\mathbf{3_2}$): Fw = 2537.25, small colorless needle, 0.28 × 0.09 × 0.05 mm^3, triclinic, *P*-1 (no. 2), a = 14.1218(3), b = 15.1886(3), c = 15.4437(3) Å, α = 112.681(2), β = 99.1365(17), γ = 108.1586(19)°, V = 2753.20(11) Å^3, Z = 1, D_x = 1.530 g cm^{-3}, μ = 1.939 mm^{-1}, T_{min}–T_{max}: 0.682–0.921. 43222 Reflections were measured up to a resolution of (sin $\theta/\lambda)_{max}$ = 0.62 Å^{-1}. 10705 Reflections were unique (R_{int} = 0.0232), of which 9596 were observed [$I > 2\sigma(I)$]. 862 Parameters were refined using 784 restraints. $R1/wR2$ [$I > 2\sigma(I)$]: 0.0335/0.0951. $R1/wR2$ [all refl.]: 0.0379/0.0993. S = 1.017. Residual electron density found between −0.50 and 0.68 e Å^{-3}.

(f) [(^{DMM}ESDP)Cu^{II}(H_2O)](ClO_4)$_2$ (**3a**)

All reflection intensities were measured at 110(2) K using a KM4/Xcalibur (detector: Sapphire3) with enhance graphite-monochromated Mo *K*α radiation (λ = 0.71073 Å) under the program CrysAlisPro (Version 1.171.36.24 Agilent Technologies, 2012). The program CrysAlisPro (Version 1.171.36.24 Agilent Technologies, 2012) was used to refine the cell dimensions. Data reduction was done using the program CrysAlisPro (Version 1.171.36.24 Agilent Technologies, 2012). The structure was solved with the program SHELXS-2013 (Sheldrick, 2013) and was refined on F^2 with SHELXL-2013 (Sheldrick, 2013). Analytical numeric absorption corrections based on a multifaceted crystal model were applied using CrysAlisPro (Version 1.171.36.24 Agilent Technologies, 2012). The temperature of the data collection was controlled using the system Cryojet (manufactured by Oxford Instruments). The H atoms were placed at calculated positions using the instructions AFIX 23, AFIX 43 and AFIX 137 with isotropic displacement parameters having values 1.2 or 1.5 times *U*eq of the attached C atoms. The H atoms attached to O1 (coordinated water molecules) were found from difference Fourier maps, and their

coordinates were refined freely (the O–H and H···H distances were restrained using DFIX instructions). The structure is mostly ordered. One of the two perchlorate counterions is found to be disordered over two orientations, and the occupancy factor of the major component of the disorder refines to 0.583(6).

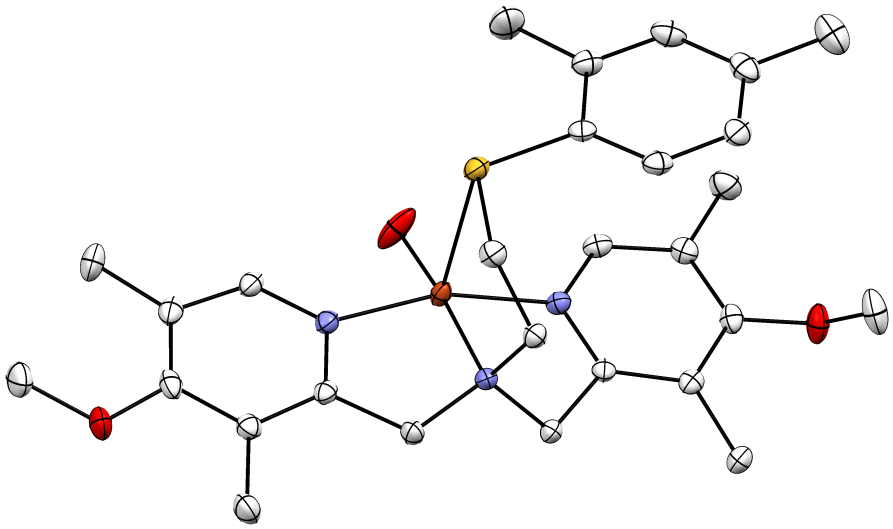

Figure S6. Displacement ellipsoid plot (50% probability level) of **3a** at 110(2) K. The H atoms and the counterions are omitted for the sake of clarity. [(^{DMM}ESDP)Cu^{II}(H_2O)](ClO_4)$_2$ (**3a**): Fw = 760.12, blue rod, 0.44 × 0.11 × 0.08 mm^3, monoclinic, $P2_1/n$ (no. 14), a = 11.0119(2), b = 26.6898(6), c = 11.0783(2) Å, β = 93.1668(19)°, V = 3251.00(11) Å^3, Z = 4, D_x = 1.553 g cm^{-3}, μ = 0.963 mm^{-1}, T_{min}–T_{max}: 0.813–0.943. 41580 Reflections were measured up to a resolution of (sin $\theta/\lambda)_{max}$ = 0.65 Å^{-1}. 7483 Reflections were unique (R_{int} = 0.0504), of which 6250 were observed [$I > 2\sigma(I)$]. 475 Parameters were refined using 73 restraints. $R1/wR2$ [$I > 2\sigma(I)$]: 0.0329/0.0773. $R1/wR2$ [all refl.]: 0.0436/0.0812. S = 1.020. Residual electron density found between –0.34 and 0.38 e Å^{-3}.

2. VT-NMR of [(^{DMM}ESE)Cu^{I}](B(C_6F_5)$_4$) (1)

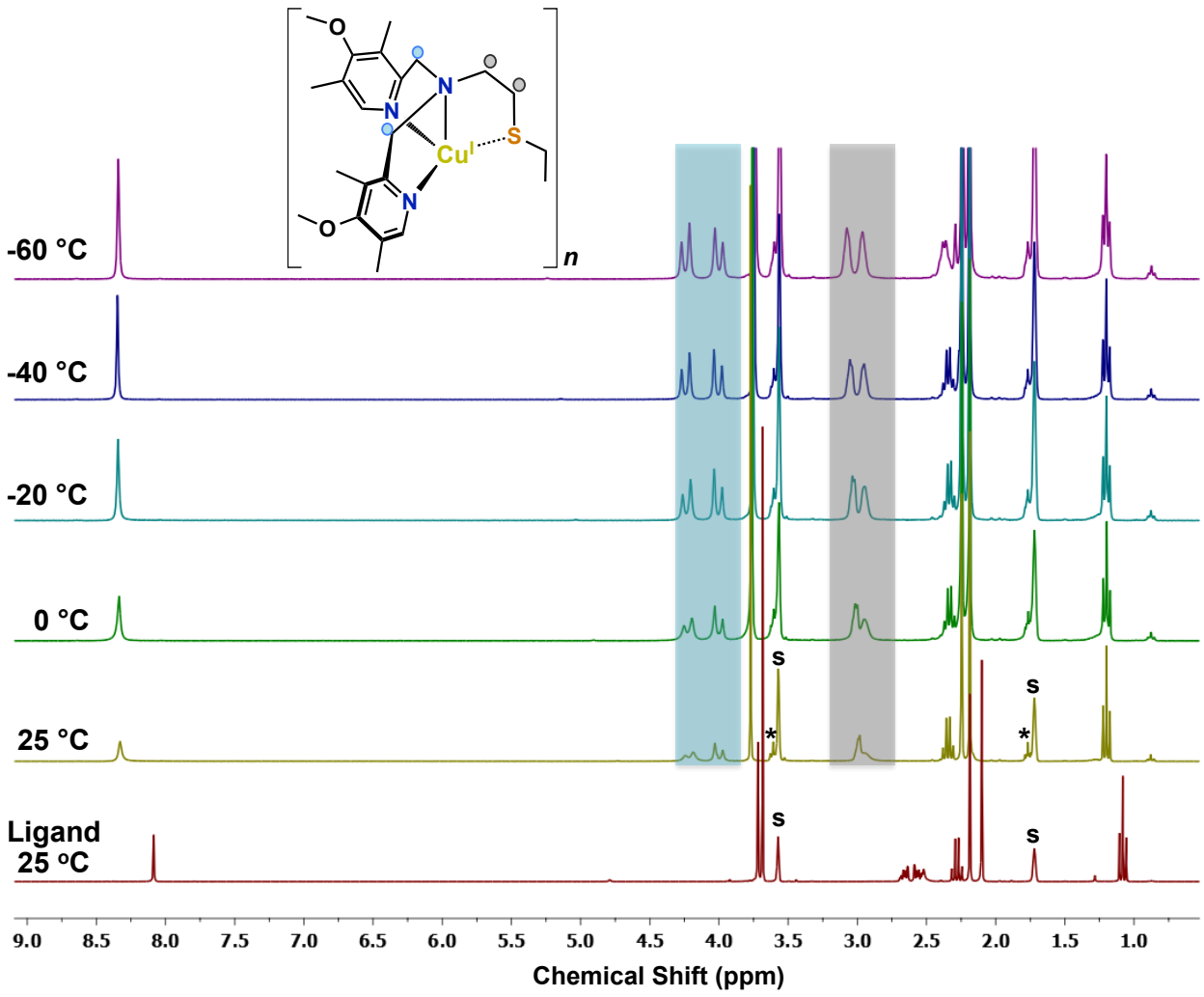

Figure S7. The ^{1}H-NMR spectrum of the free ^{DMM}ESE ligand and variable-temperature ^{1}H-NMR spectra of [(^{DMM}ESE)Cu^{I}](B(C_6F_5)$_4$) (**1**) (THF-d_8, 300 MHz) ("s" denotes peaks due to residual hydrogen atoms in the solvent; * indicates THF impurity in the Cu(I) precursor). There are a few small but distinctive changes in the VT-^{1}H-NMR spectra of **1**, but these can be ascribed to simpler dynamic behavior (as is well known for copper ion complexes).[1-7] (i) A rapid interchange process, with delegation of the S(thioether) atom, would result in the observation of inequivalent proton resonances for the N-CH_2CH_2-S- moiety at lower temperatures (exhibiting a clear doublet) but collapse to a singlet at RT, as observed, (gray region). As an aside, the blue region highlights the signal(s) for the N-CH_2-pyridyl moiety, where a typical geminal coupling results in a doublet signal for the two hydrogen atoms now in inequivalent chemical environments, due to copper(I) coordination. This methylene group is a simple singlet in the ^{1}H-NMR spectrum of the free ^{DMM}ESE ligand**.**

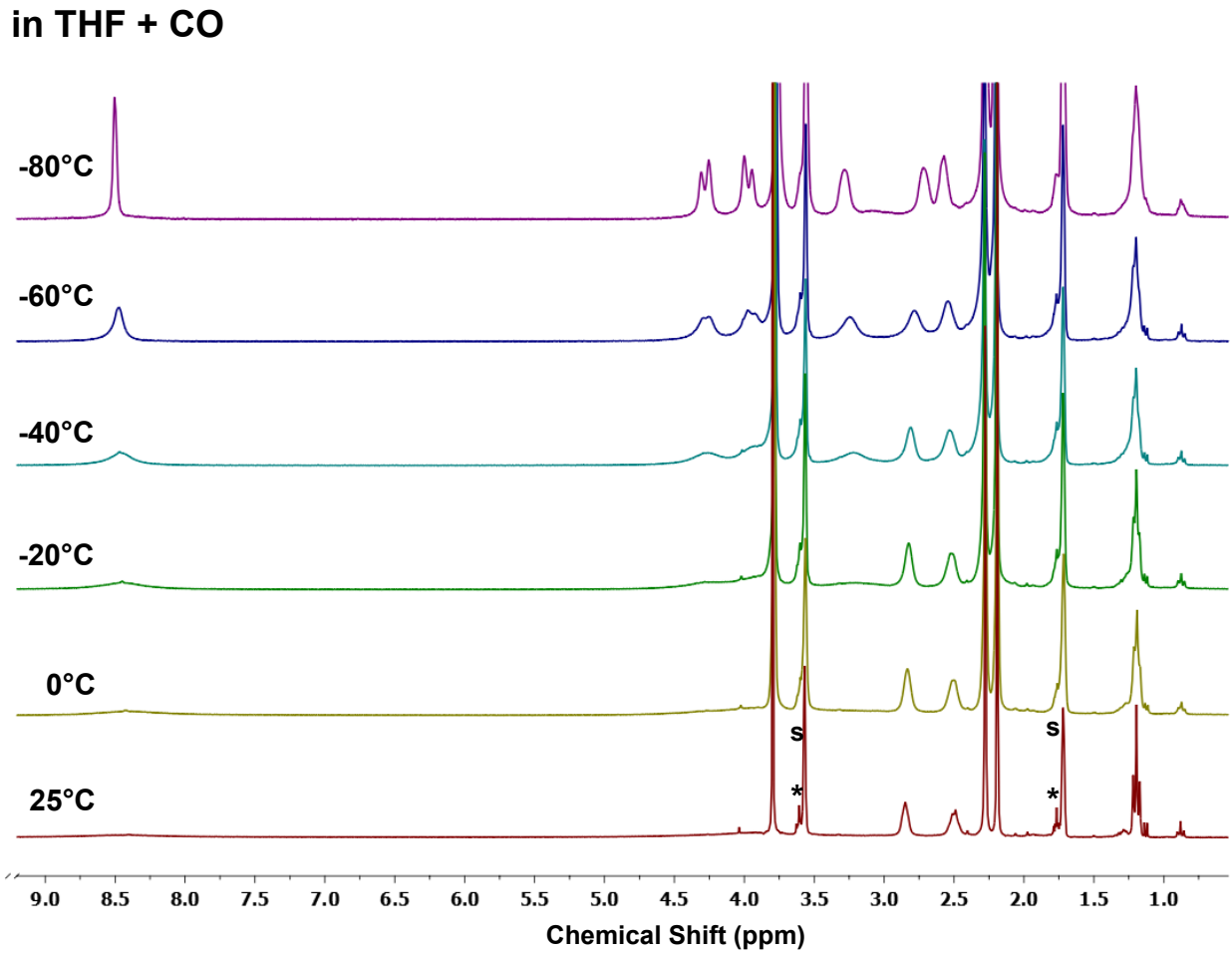

Figure S8. VT ^{1}H-NMR (300 MHz, THF-d_8) data of [(^{DMM}ESE)Cu^{I}](B(C_6F_5)$_4$) **(1)** + CO ("s" denotes peaks due to residual hydrogen atoms in the solvent; * indicates THF impurity in the Cu(I) precursor).

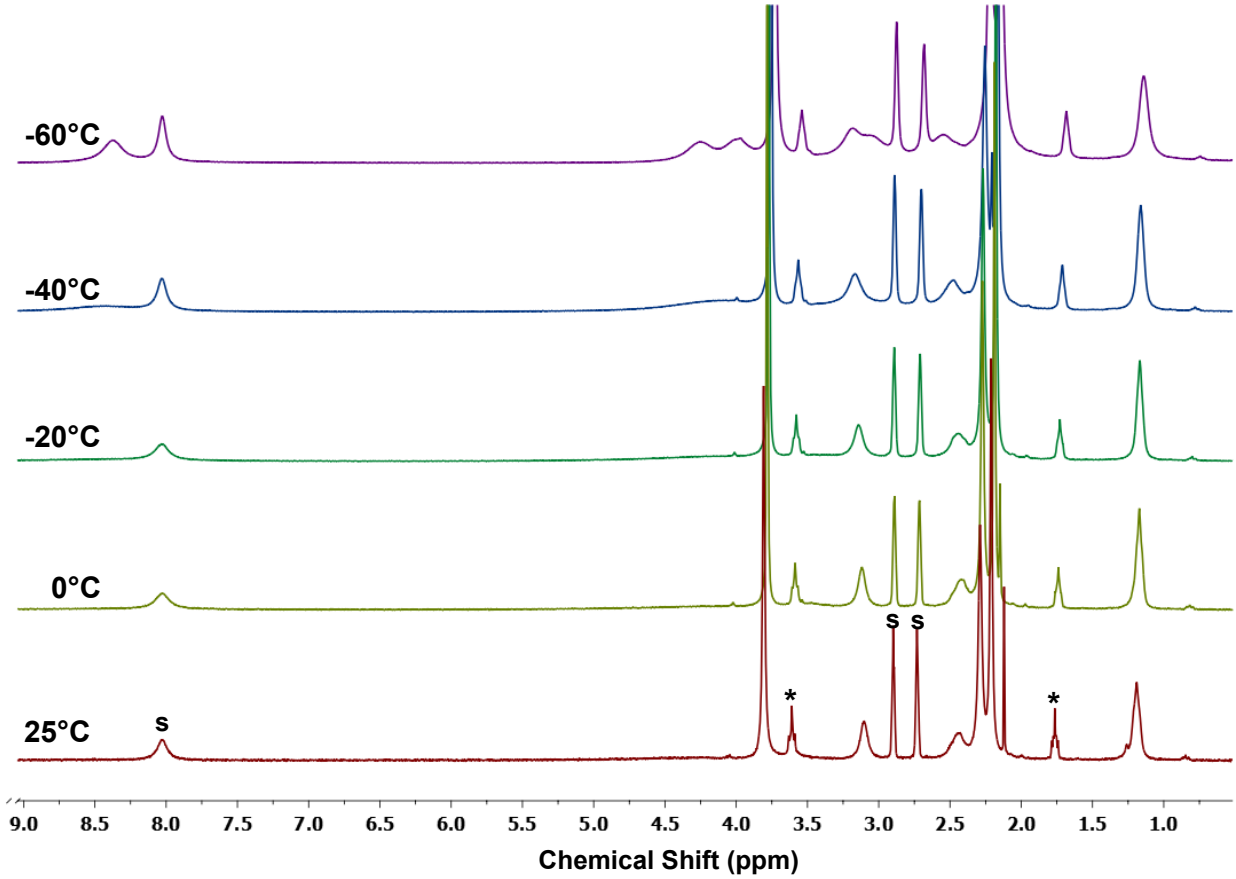

Figure S9. VT ^{1}H-NMR (300 MHz, DMF-d_7) data of [(^{DMM}ESE)Cu^{I}](B(C_6F_5)$_4$) **(1)** ("s" denotes peaks due to residual hydrogen atoms in the solvent; * indicates THF impurity in the Cu(I) precursor).

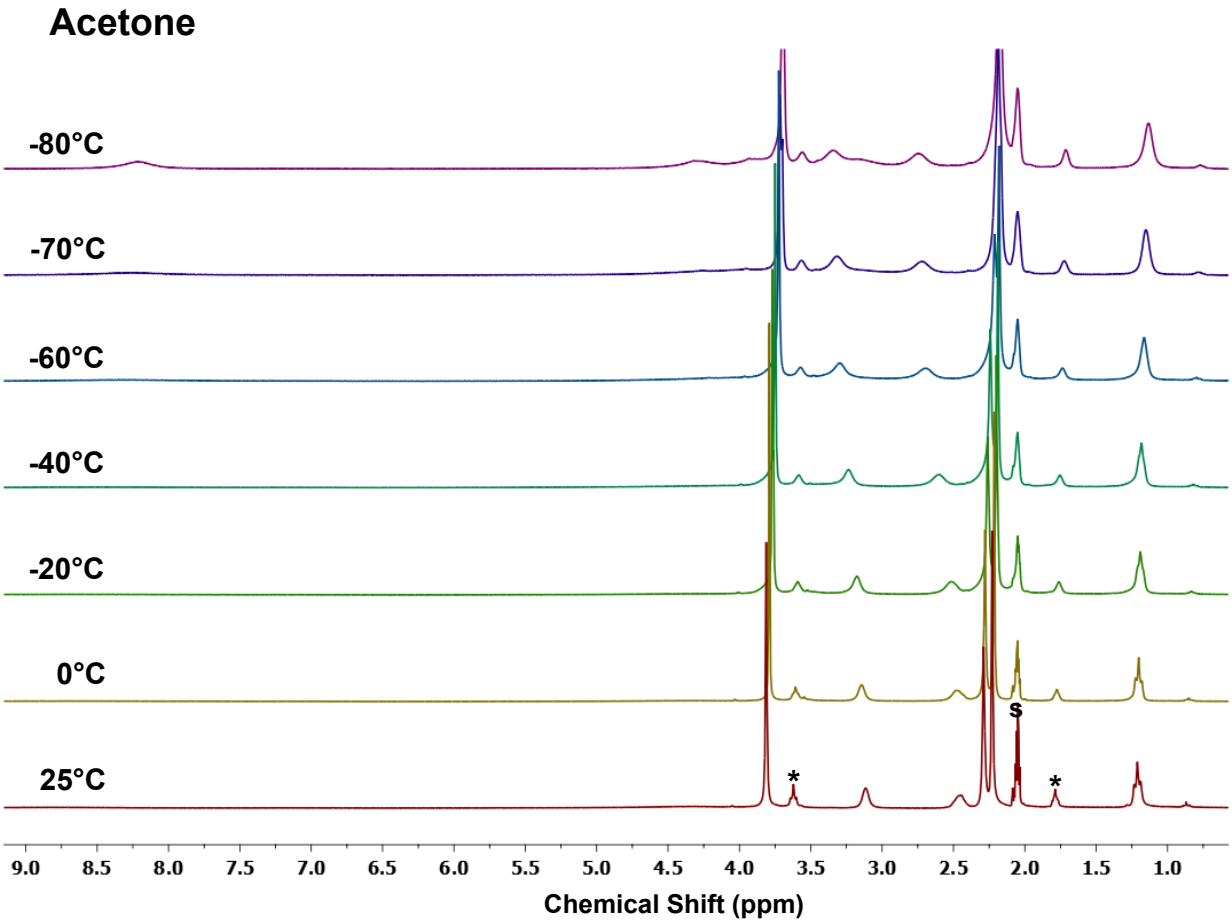

Figure S10. VT ^{1}H-NMR (300 MHz, Acetone-d_6) data of [(^{DMM}ESE)Cu^{I}](B(C_6F_5)$_4$) **(1)** ("s" denotes peaks due to residual hydrogen atoms in the solvent; * indicates THF impurity in the Cu(I) precursor).

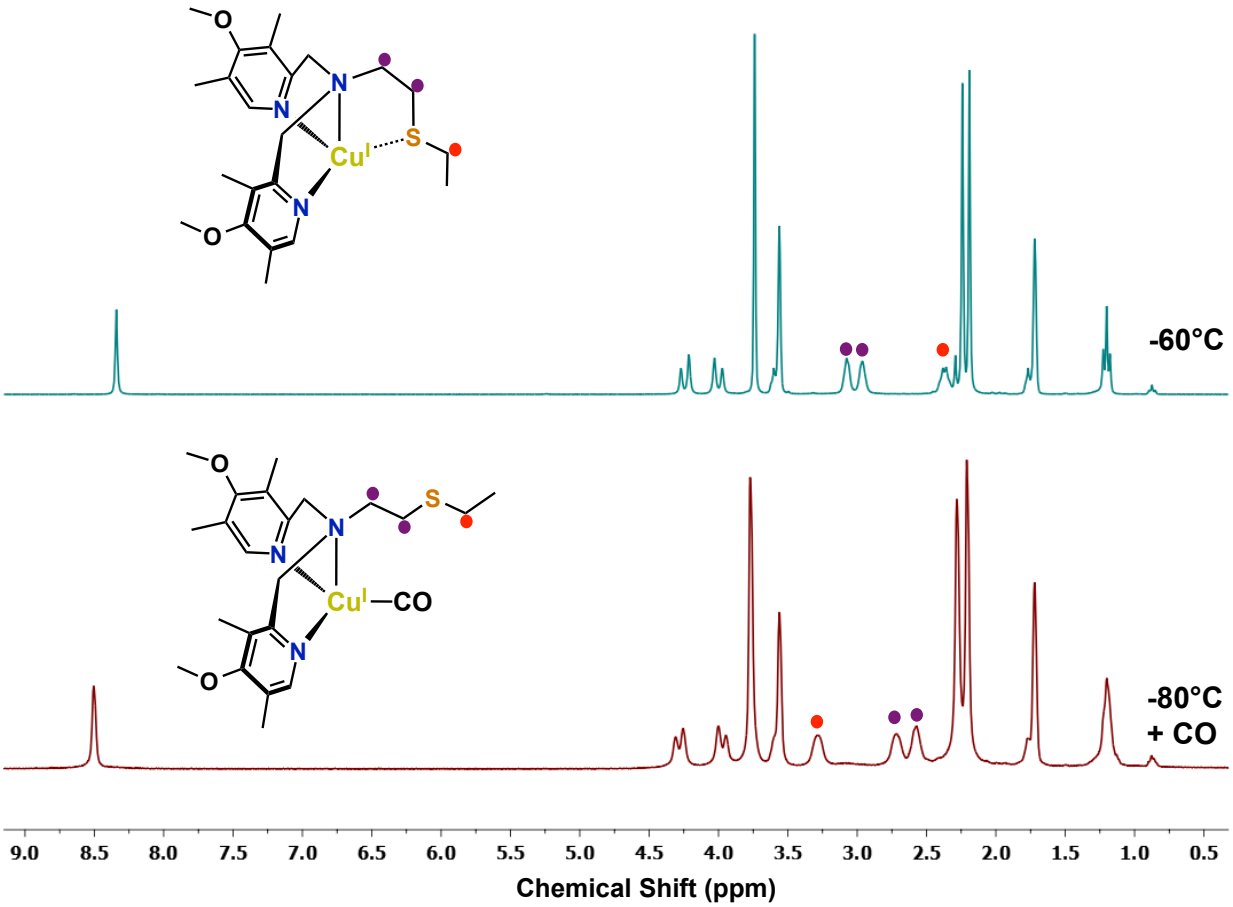

Figure S11. VT ^{1}H-NMR (300 MHz, THF-d_8) data of [(^{DMM}ESE)Cu^{I}](B(C_6F_5)$_4$) **(1)** (top) at –60 ºC and (**1**) + $CO_{(g)}$ (bottom).

3. DOSY NMR experiments

Table S1. DOSY Derived Diffusion Coefficients (*D*) of Mono- and Dinuclear Cu(I) Complexes in THF-d_8 ($D_{\text{THF-}d8} = 10^{-8.50}$ m^2s^{-1}). The NMR spectroscopic technique Diffusion Ordered Spectroscopy (DOSY) utilizes pulsed field gradients to measure the translational diffusion of molecules. The measured diffusion constant is a function of the hydrodynamic radius of the molecule, as given by the Stokes-Einstein equation.

Complex	Log $D = 10^D$ [m^2/s]	
[(^{DMM}ESE)Cu^I]$B(C_6F_5)_4$ (1)	$10^{-9.08} = 8.317 \times 10^{-10}$	Monomer
[(TMPA)Cu^I(CH_3CN)]($B(C_6F_5)_4$)	$10^{-9.07} = 8.609 \times 10^{-10}$	Monomer
[(N5)Cu^I_2]($B(C_6F_5)_4$)$_2$	$10^{-9.33} = 4.677 \times 10^{-10}$	Dinuclear
[(XYL-H)Cu^I_2]($B(C_6F_5)_4$)$_2$	$10^{-9.31} = 4.897 \times 10^{-10}$	Dinuclear

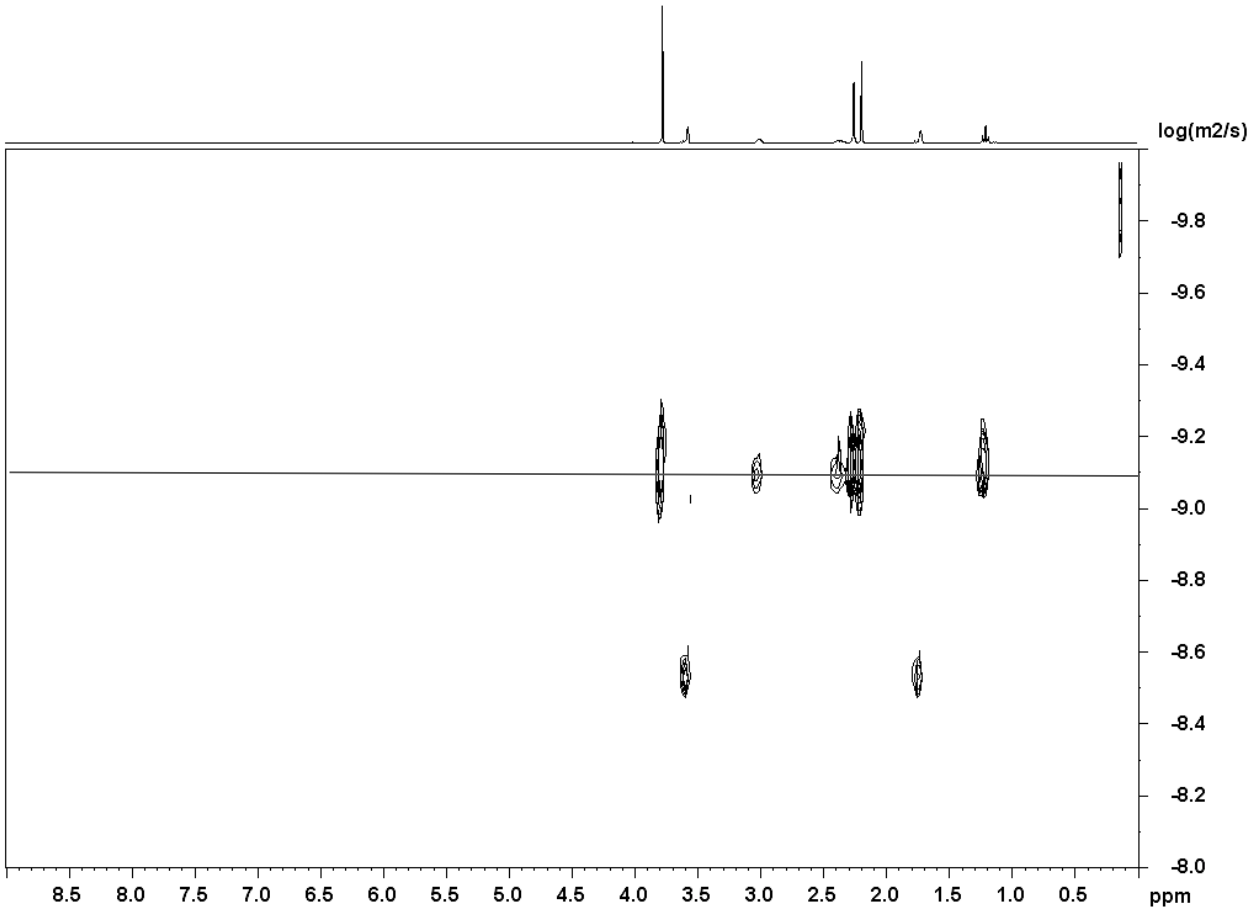

Figure S12. DOSY NMR data of [(^{DMM}ESE)Cu^I]($B(C_6F_5)_4$) **(1),** affording a diffusion coefficient (*D*) of $D = 10^{-9.08}$ m^2s^{-1} ($D_{\text{THF-d8}} = 10^{-8.50}$).

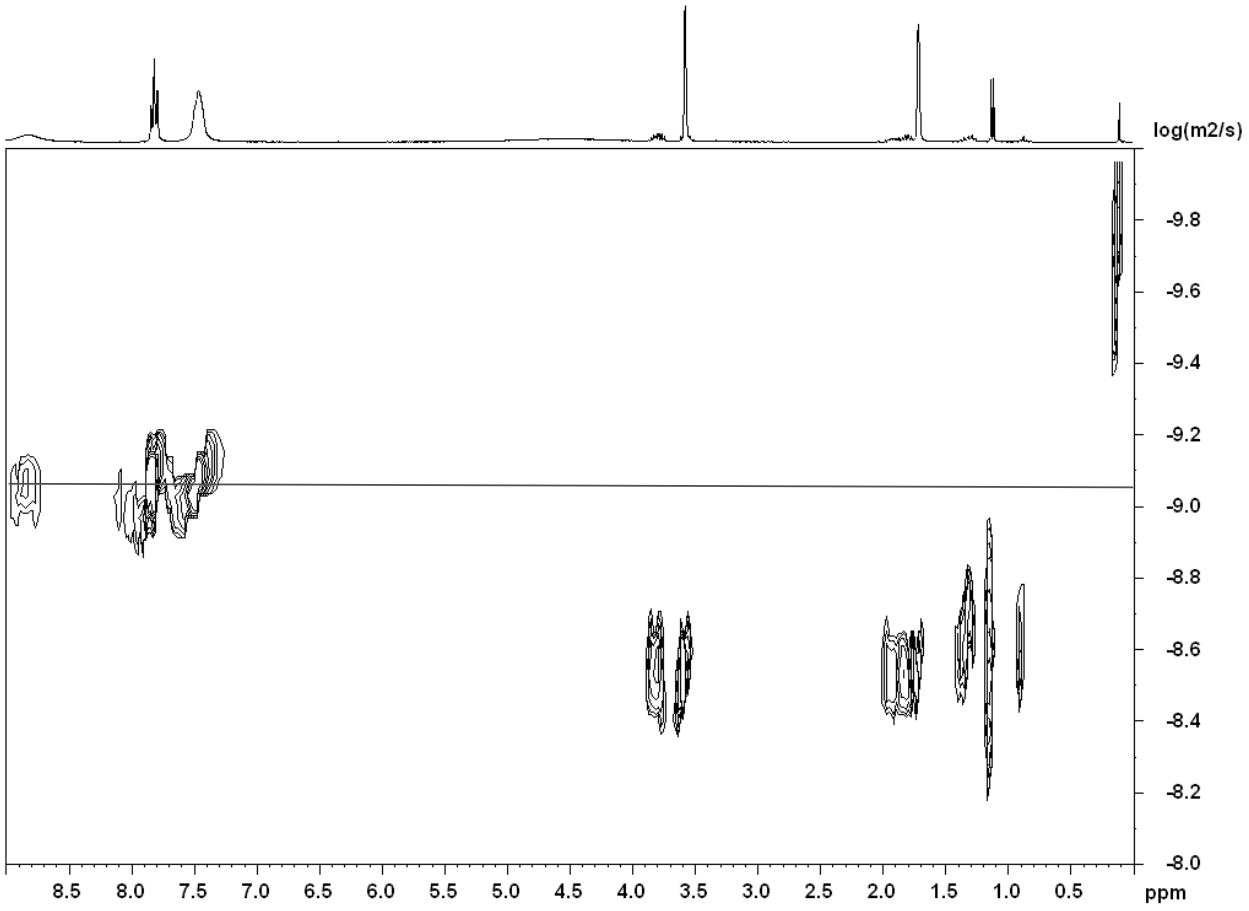

Figure S13. DOSY NMR data of $[(TMPA)Cu^{I}](B(C_6F_5)_4)$ **(1),** affording a diffusion coefficient (D) of $D = 10^{-9.065}$ m^2s^{-1} ($D_{THF\text{-}d8} = 10^{-8.50}$).

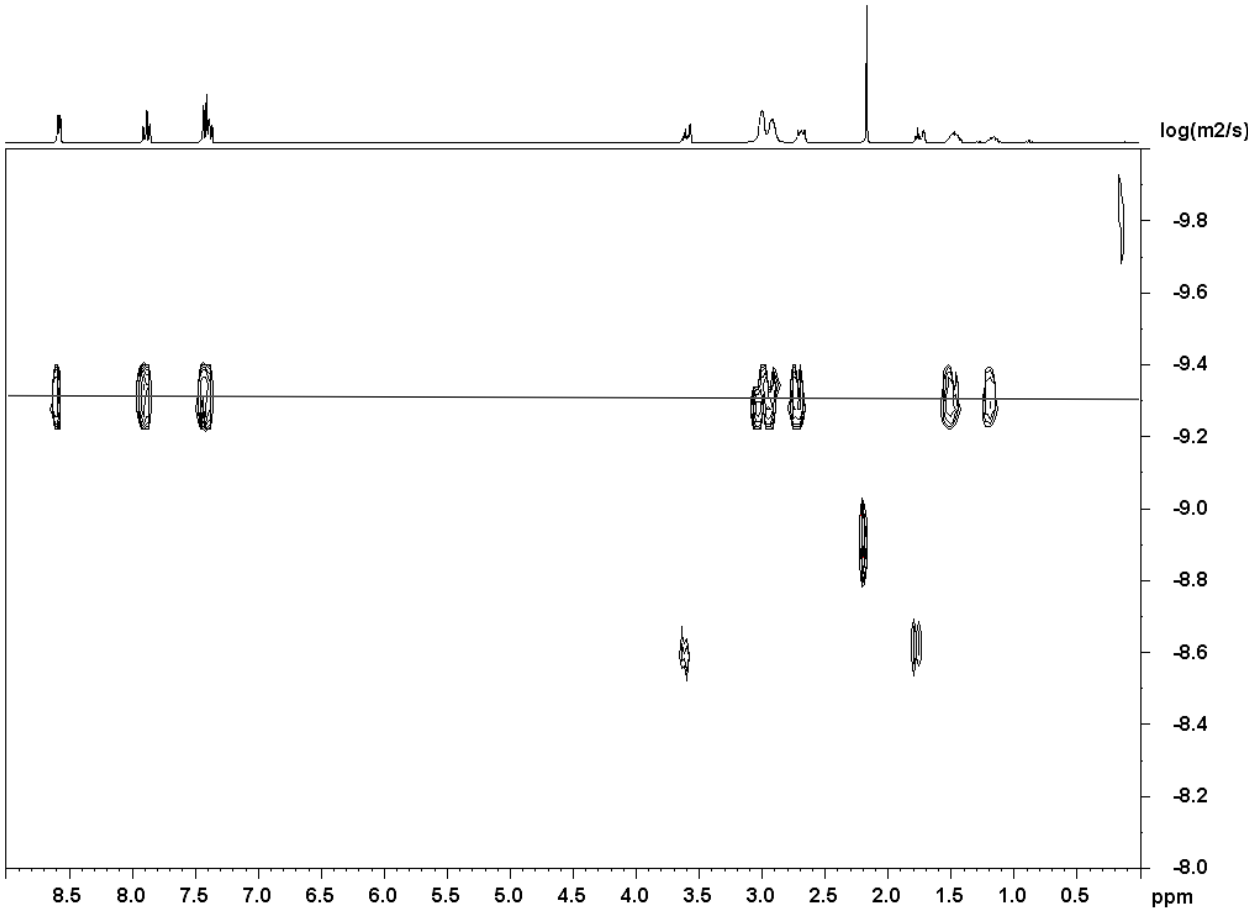

Figure S14. DOSY NMR data of $[(N5)Cu^{I}_{2}(CH_3CN)](B(C_6F_5)_4)_2$ **(1),** affording a diffusion coefficient (D) of $D = 10^{-9.33}$ m^2s^{-1} ($D_{THF\text{-}d8} = 10^{-8.50}$).

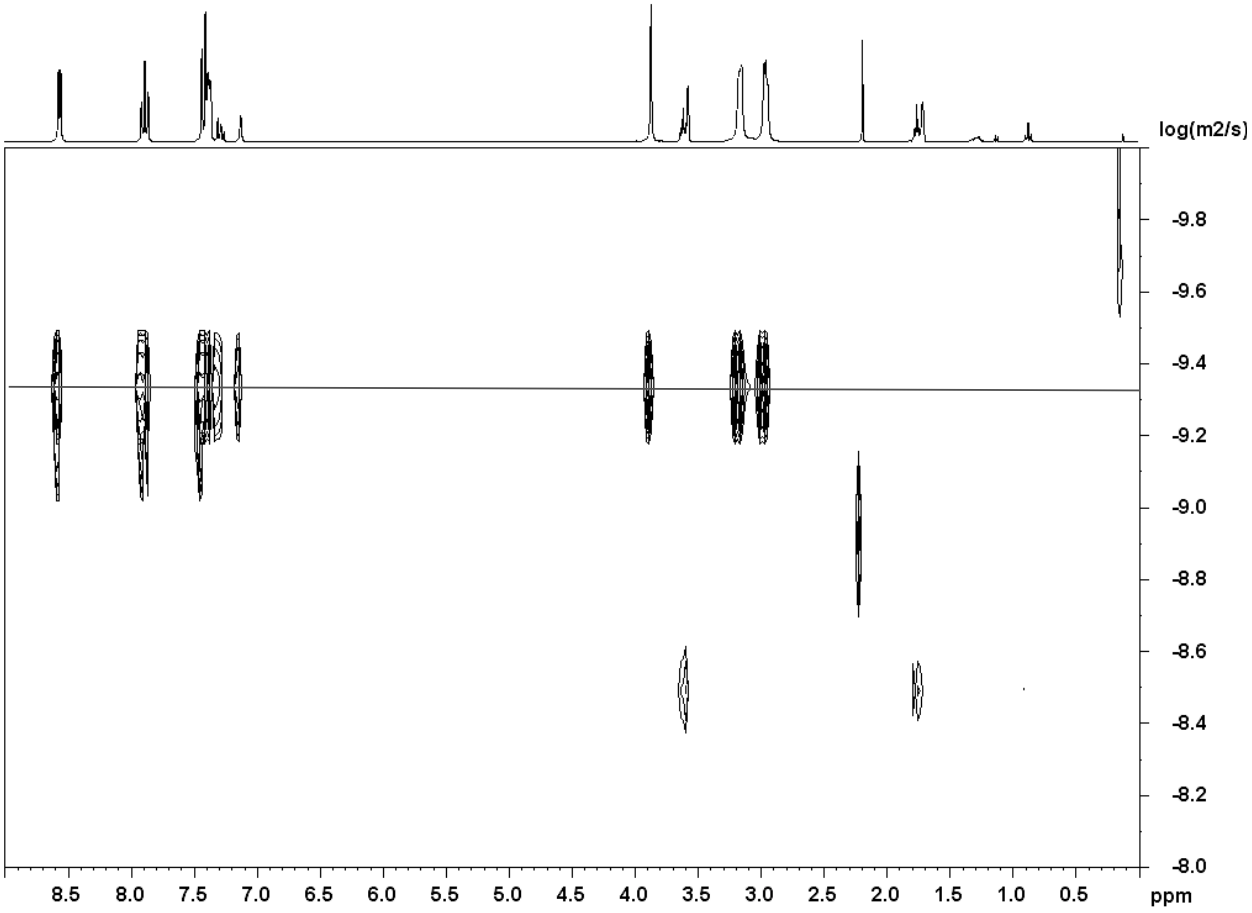

Figure S15. DOSY NMR data of $[(XYL\text{-}H)Cu^{I}_{2}](B(C_6F_5)_4)_2$ **(1),** affording a diffusion coefficient (D) of $D = 10^{-9.31}$ m^2s^{-1} ($D_{THF\text{-}d8} = 10^{-8.50}$).

4. CO Binding of Copper(I) Complexes and Electrochemical Comparisons

To obtain further insights into the solution state behavior of copper(I) complexes, examined ligand-Cu(I)-CO infrared spectra and ligand-Cu(II) electrochemical behavior. Both of these techniques afford information concerning the relative amount of electron donation provided to the copper(I) ions as a function of the ligand sets studied here. Cu(I)-CO complexes were in situ by bubbling excess $CO_{(g)}$ into acetonitrile solutions of **1**, **2** and **3** and IR spectra were recorded. The IR spectra revealed ν_{CO} vibrations at 2089, 2090 and 2090 cm^{-1} respectively (see **Table S2**). These values are almost identical to those of both $[(ESE)Cu^{I}(CO)]^{+}$ and $[(TMPA)Cu^{I}(CO)]^{+}$, where the potentially tetradentate TMPA (tris-2-pyridylmethyl)-amine) ligand provides only tridentate (*i.e.*, N_3) coordination.[8,9] Thus, we propose that all three N_3S chelates studied here behave as "tridentate" donors in the presence of CO in solution, with the thioether not coordinated, which explains the thus indicating similar electronic environment of the copper complexes as indicated by IR spectroscopy.

However, there is some variation in the effective electron density at copper ion in these complexes, as shown by their electrochemical behavior in CH_3CN (via cyclic voltammetry, **Table S2**).[8] The reduction potential for the three DMM derived ligands are similar and approximately 110 mV lower than ESE, which contains pyridine donors due to the increased donor strength of the *p*-methoxy group leading to more negative Cu^{II}/Cu^{I} redox potentials (**Table S2**). The slightly more negative $E_{½}$ value for **1a** compared to **2a** and **3a** indicates that the ethylthio arm of **1a** is a marginally better donor than the thiophenyl-type arms in **2a** and **3a**.

Table S2. IR Spectroscopic Data for ligand-Cu(I)-CO Complexes; Cyclic Voltammetric Data for Ligand-Cu Complexes in CH_3CN.

	PHM[a]	DβM[a]	TMPA[b]	^{DMM}ESE[b]	^{DMM}ESP[b]	^{DMM}ESDP[b]	ESE[b]
ν_{CO} (cm^{-1})	2093	2089	2092[c,d] 2073[c]	2089[d]	2090[d]	2090[d]	2094[d]
$E_{½}$ (mV)[e]	—	—	–420	–370	–360	–350	–250

[a] Data for protein Cu_M sites, with His_2Met coordination.[10,11] [b] Ligand-Cu(II) complexes were employed for cyclic voltammetric measurements. [c] Measured in THF.[8] [d] Ligand-Cu(I) complexes employed for measurements. We can conclude that $[Cu^{I}(CH_3CN)_4]^{+}$ is not forming. Separately with determined that $[Cu^{I}(CH_3CN)_4](B(C_6F_5)_4$ bubbled with CO in CH_3CN solvent gives rise to ν_{CO} = 2020 cm^{-1}. [e] mV *vs*. $[Fe(Cp)_2]^{+/0}$

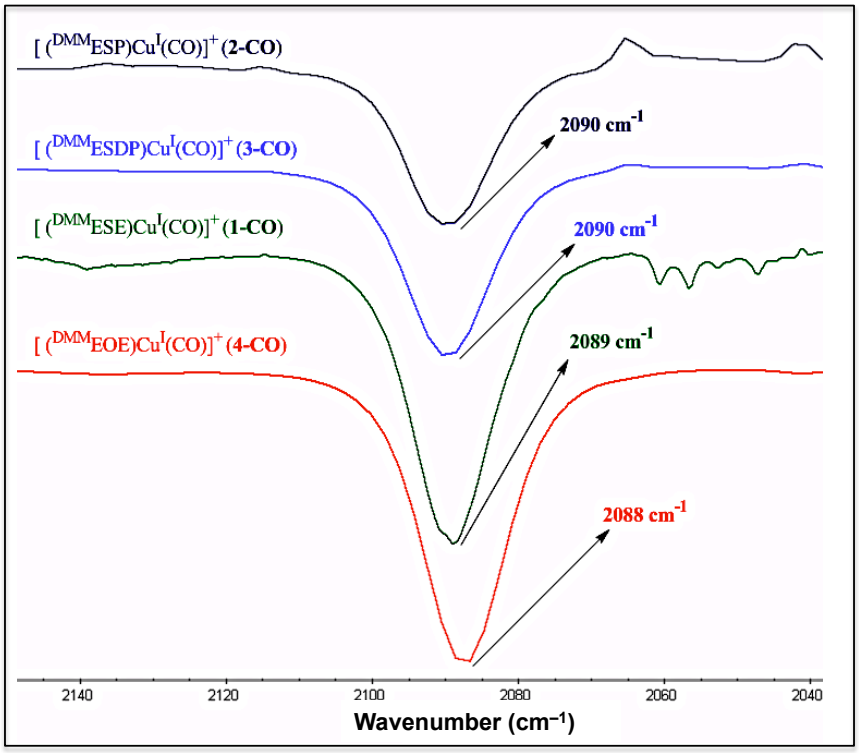

Figure S16. Solution IR spectra of ligand-Cu(I)-CO complexes in acetonitrile at room temperature. All of the steps described in this section were done at room temperature. Dissolving complex **1**, **2**, **3**, and **4** in acetonitrile and treating with excess $CO_{(g)}$ generated **1-CO**, **2-CO**, **3-CO**, and **4-CO**, respectively. In the glove box, the desired copper(I) complex (**1**, **2**, **3**, or **4**) was dissolved in acetonitrile such that the concentration is 4 ~ 5 mM. A tiny aliquot of the copper(I) complex/acetonitrile stock solution was transferred to a IR flow cell and sealed with Precision Seal® rubber septa caps. Immediately, the IR flow cell was removed from the glove box and mounted on a Nexus 670 FT-IR instrument. The IR spectrum of the dissolved copper(I) complex obtained was taken as the background. Compressed carbon monoxide (CO) gas was bubbled through a syringe needle into the IR flow cell. Another syringe needle with an outlet to the atmosphere was used to relieve the pressure. After bubbling for 45 seconds, both the outlet syringe needle and the needle providing the $CO_{(g)}$ were immediately removed. The *in situ* ligand-Cu(I)-CO adduct (**1-CO**, **2-CO**, **3-CO**, or **4-CO**) was quickly mounted on a Nexus 670 FT-IR instrument and the spectrum was recorded. **Figure S9** summarizes the ν(C-O) stretches obtained.

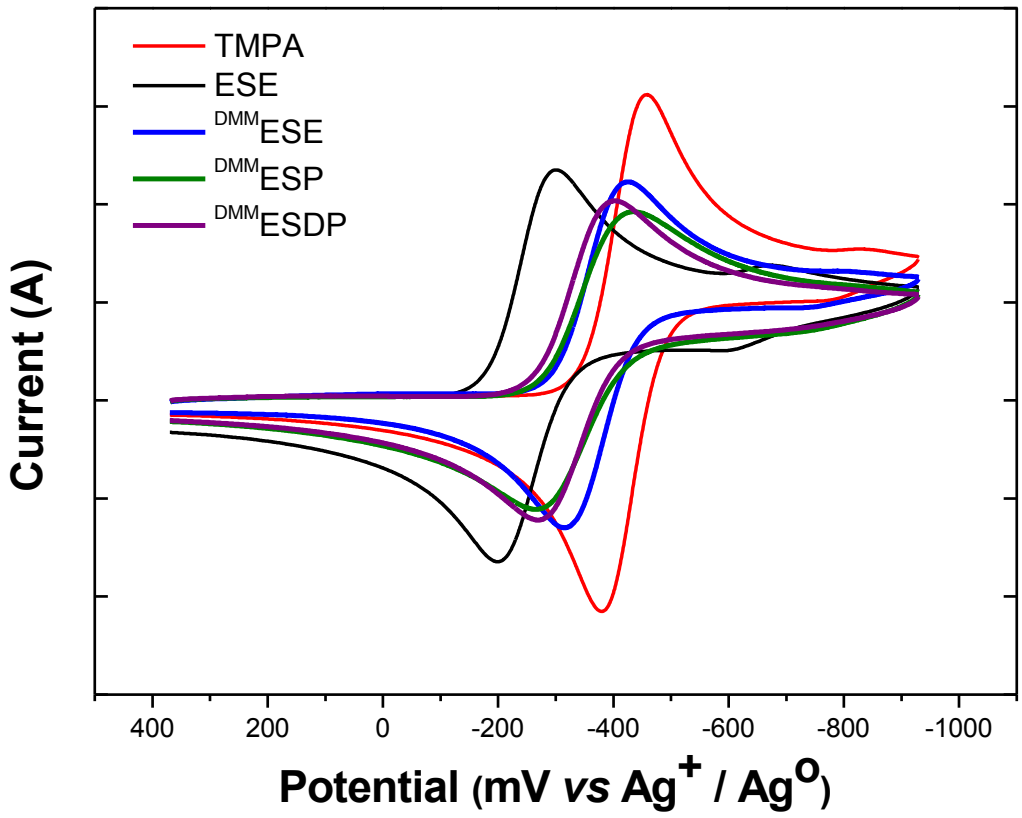

Figure S17. Cyclic voltammetry data for copper(II) complexes in CH_3CN (mV *vs*. $[Fe(Cp)_2]^{+/0}$). Ligand-Cu(II) complexes (~ 1 mM) were employed for cyclic voltammetric measurements. CV measurements were undertaken in freshly distilled acetonitrile using a BAS 100B electrochemical analyzer with a glassy carbon working electrode and a platinum wire auxiliary electrode. Potentials were recorded versus a $Ag/AgNO_3$ electrode. The voltammograms are plotted *versus* the $Fe(Cp)_2^{+/0}$ potential which was measured as an external standard. Scans were run at 50−200 mV/s under Ar atmosphere using ca. 0.1 M $(Bu_4N)(PF_6)$ as the supporting electrolyte.

5. EPR experiments

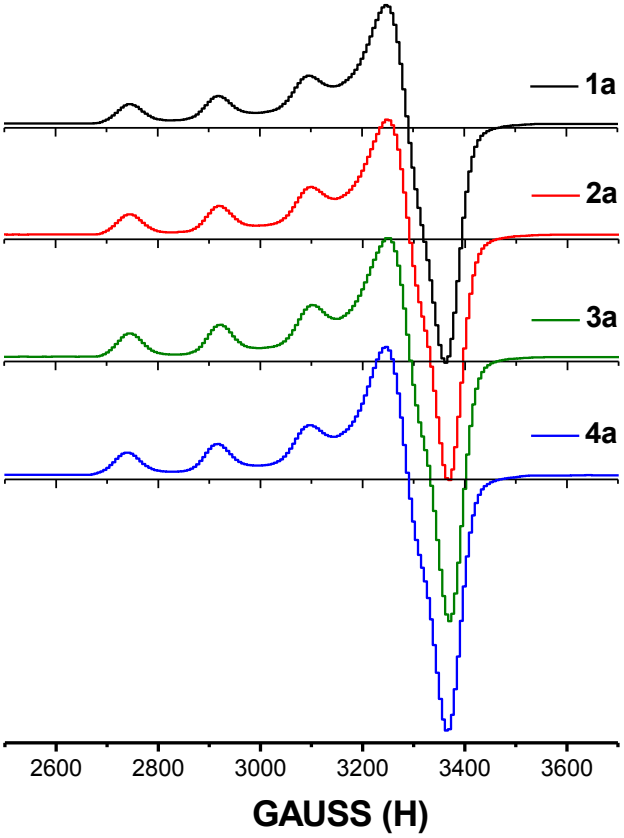

Figure S18. EPR spectra of **1a** ($g_{\|}$ = 2.263, $A_{\|}$ = 168 G, $g\perp$ = 2.036), **2a** ($g_{\|}$ = 2.263, $A_{\|}$ = 168 G, $g\perp$ = 2.034), **3a** ($g_{\|}$ = 2.262, $A_{\|}$ = 168 G, $g\perp$ = 2.034) and **4a** ($g_{\|}$ = 2.265, $A_{\|}$ = 170 G, $g\perp$ = 2.036) taken with an X-band spectrometer (ν = 9.186 GHz) in acetone at 70 K. Copper(II) complex concentrations: 2 mM.

6. Control experiments

A Schlenk cuvette was charged with 2.5 mL of a 0.25 mM solution of [(^{DMM}ESP)Cu^{I}]($B(C_6F_5)_4$) in MeTHF. The cuvette was sealed with a septum and secured with a plastic zip tie. This cell was transferred to the pre-cooled cryostat and allowed to chill with a minimum of 10 minutes allowed for equilibration prior to oxygenation. Oxygenation of the copper samples was achieved by slowly bubbling dioxygen through the solution with a Hamilton gastight syringe from –80 °C to –135 °C. Both species, a trans-peroxo dicopper(II) (**2^{P}**) and bis-μ-oxo dicopper(III) (**2^{O}**) were generated simultaneously and then decomposed from –80 °C to –135 °C.

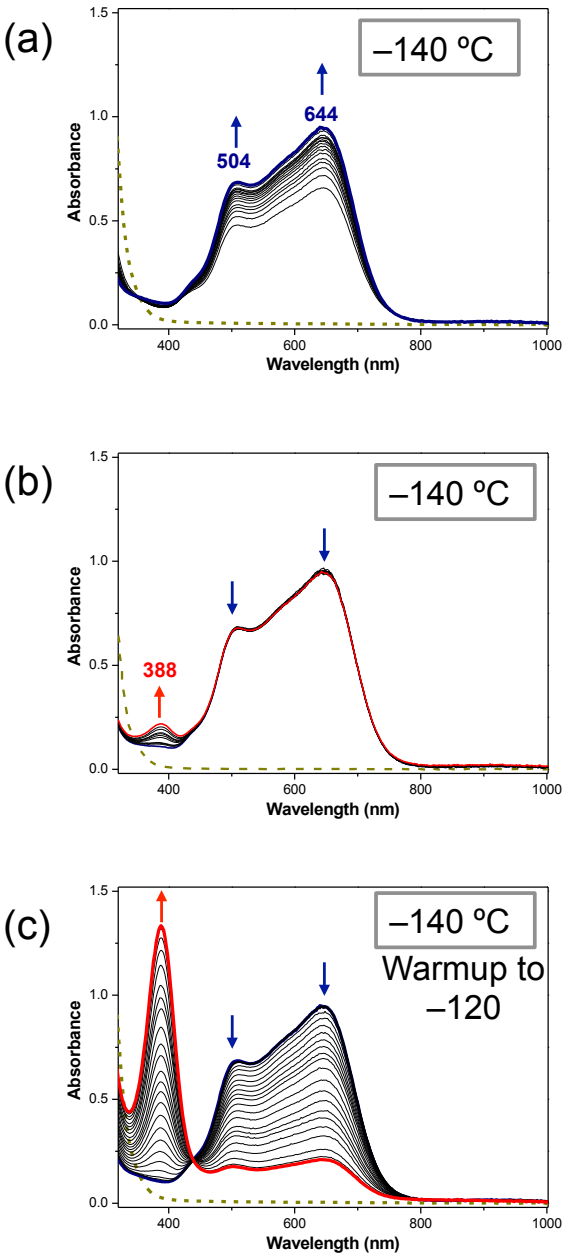

Figure S19. UV-vis data of the reaction of **2** with dioxygen in cyclopentyl methyl ether (CPME) (a) formation of $\mathbf{2^P}$ in –140 ºC, (b) after 30 min, and (c) warmed up from –140 °C to –120 °C and then recorded as a function of time, ~10 min. Using CPME as solvent allows us to go to –140 °C. In spectrum (a) we observe with time (< 19 min.) full formation of the trans peroxo complex ($\mathbf{2^P}$) (504 & 644 nm). However, after 30 min. we see a very small amount of bis-mu-oxo complex $\mathbf{2^O}$ forming, i.e., the conversation is starting to occur. But it is very slow, and so warming to –120 °C, shown is (c), shows the nearly complete conversion of $\mathbf{2^P}$ to $\mathbf{2^O}$, but notice that there always remains some amount of $\mathbf{2^P}$, even after long times. This behavior can only be ascribed to an equilibrium process, where perturbing the system by warming, there is a shift from mostly or nearly all $\mathbf{2^P}$ to mostly $\mathbf{2^O}$.

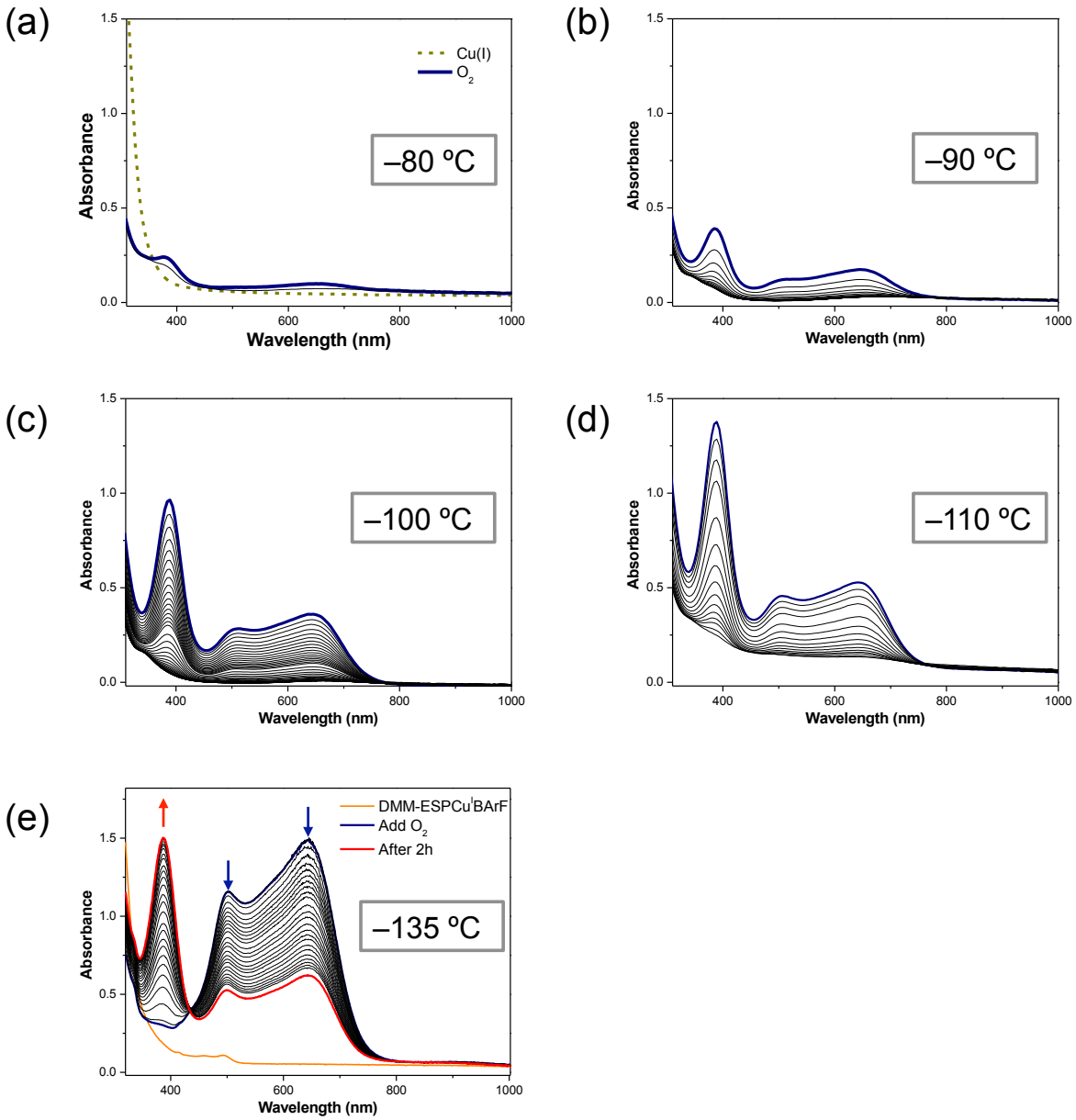

Figure S20. UV-vis data of the reaction of **2** with dioxygen in MeTHF (a) –80 °C, (b) –90 °C, (c) –100 °C, (d) –110 °C, and (e) –135 ºC. This series of spectra (and those in **Figure S19**) demonstrate that trans-peroxo dicopper(II) complex $\mathbf{2^P}$ and bis-μ-oxodicopper(III) species $\mathbf{2^O}$, are in (dynamic) equilibrium. In (a), both complexes are unstable, and have already decomposed (with loss of their characteristic charge-transfer bands) following oxygenation and recording of a first spectrum (on the benchtop), ~10 s later. In (b), (c) and (d), both $\mathbf{2^P}$ and $\mathbf{2^O}$ form but to a small extent (but more is formed as the temperature is lowered), and then decompose. It is apparent that the ratio of $\mathbf{2^O}$ to $\mathbf{2^P}$ changes with temperature. In (e) this conclusion is even more apparent; in the first spectrum recorded (at –135 °C) (blue spectrum), there is a large amount of trans peroxo formed, and almost no $\mathbf{2^O}$ is present (λmax = 388 nm), but with time, ~ 2 hours, $\mathbf{2^P}$ is depleted at the expense of $\mathbf{2^O}$. And at this temperature no decomposition is apparent over this time period, as is seen in those spectra recorded at higher temperature, spectra (a)-(c).

7. The natural decomposition of 2^{P} and 2^{O}.

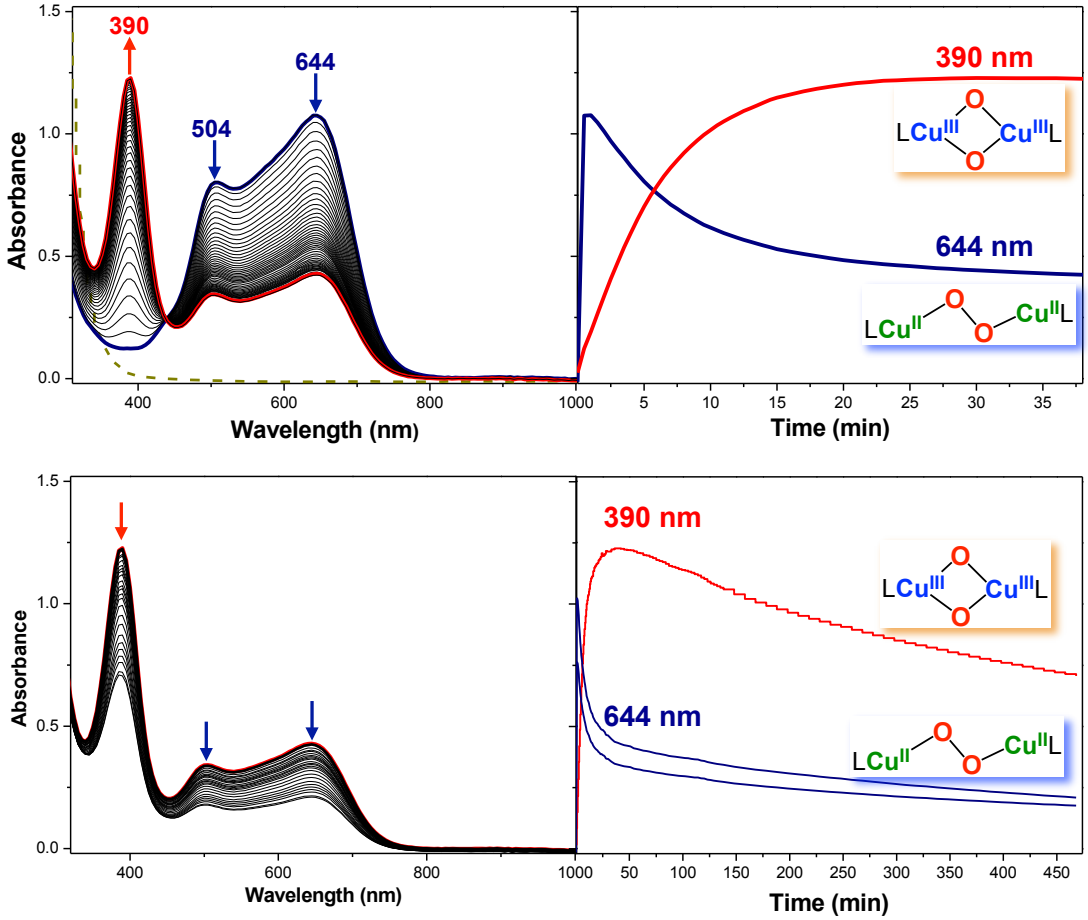

Figure S21. UV-vis data and time profiles for the equilibrium of $\mathbf{2^{P}}$ and $\mathbf{2^{O}}$ and the natural decomposition of both species in MeTHF at -130 ^{o}C for ~ 8 hours.

8. The reaction of 2^{P} with anions.

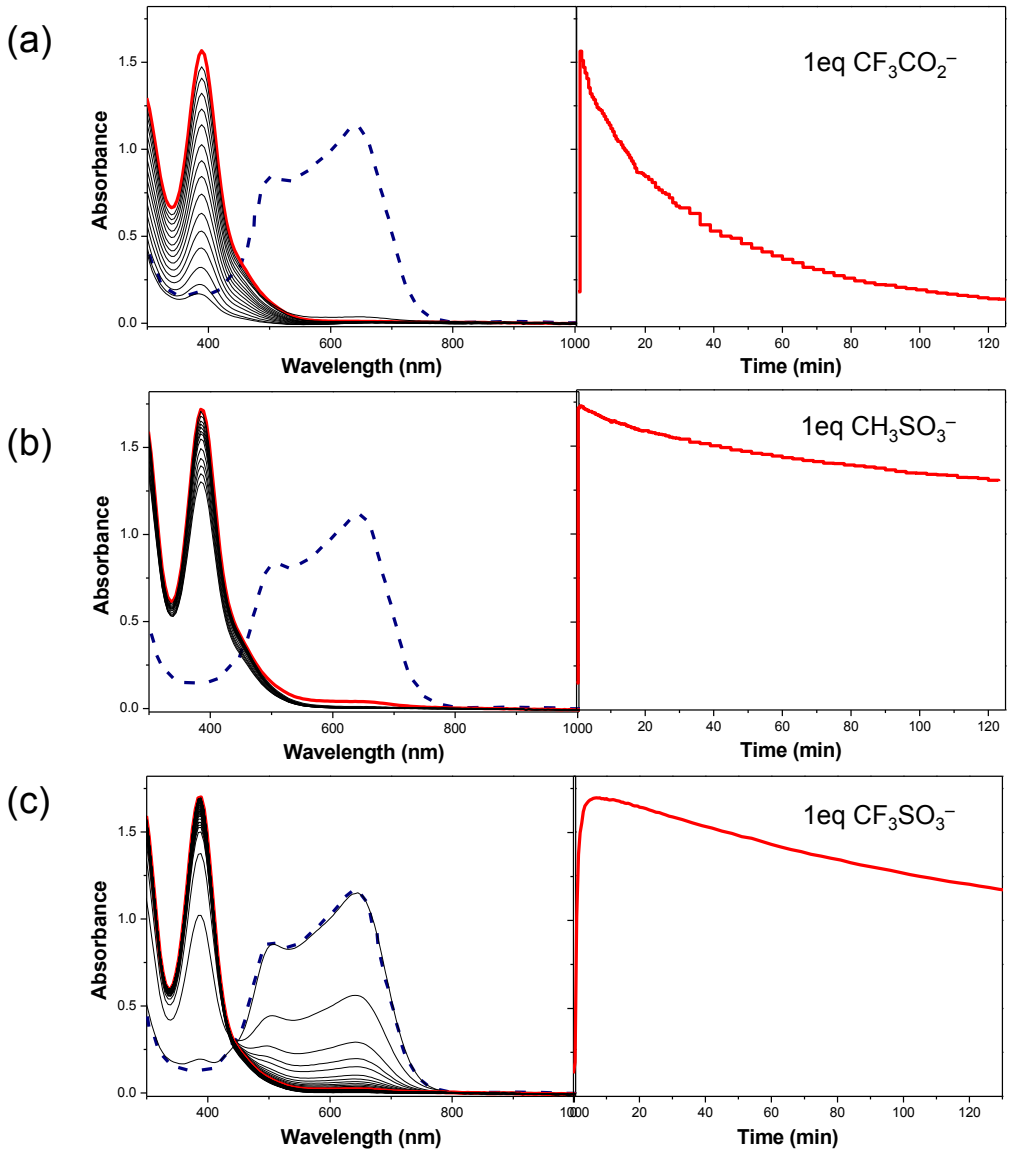

Figure S22. UV-vis data of the reaction of $\mathbf{2^{P}}$ with (a) 1eq $CF_3CO_2^-$, (b) 1eq $CH_3SO_3^-$ and (c) 1eq $CF_3SO_3^-$ form a pure bis-μ-oxo species ($\mathbf{2^{O}}$)-(anion) in MeTHF at –130 °C.

9. UV-vis spectra of 1^{P}, 3^{O} and 4^{O} species

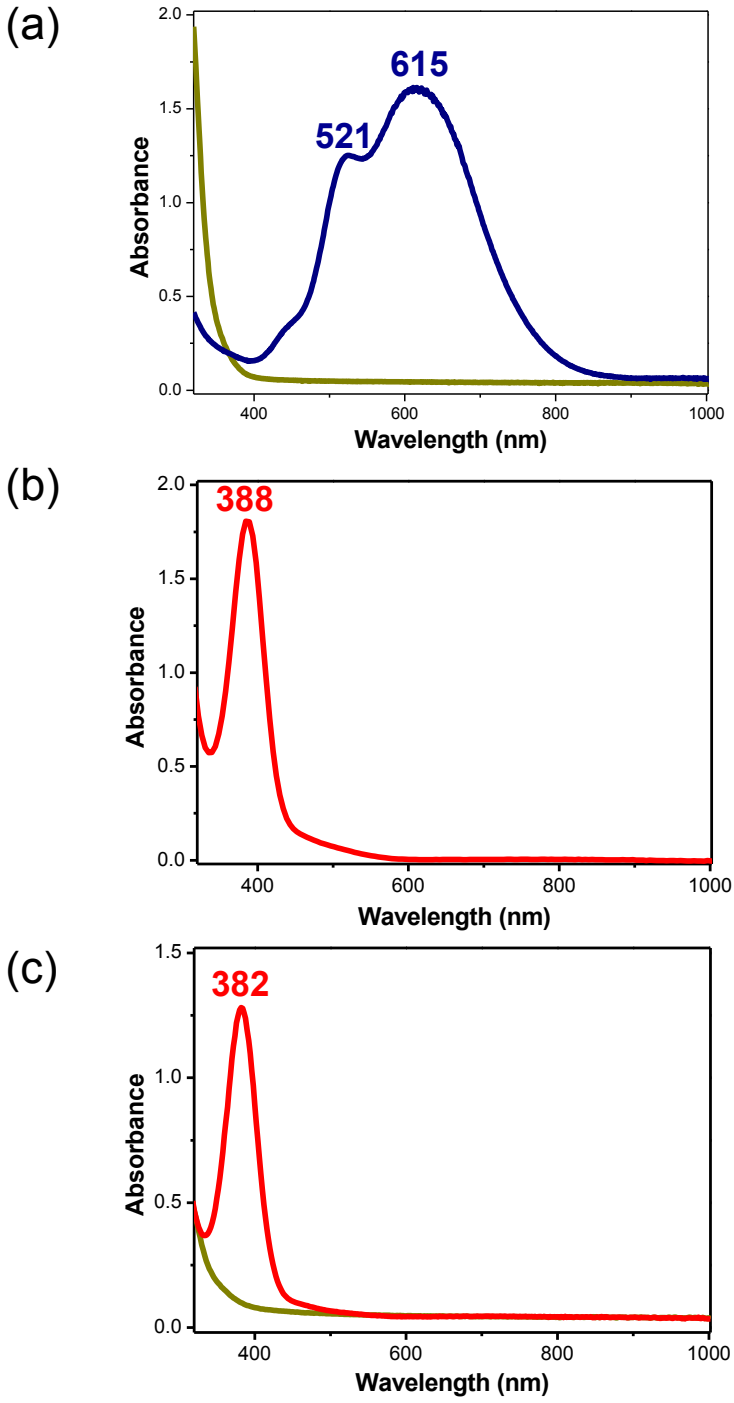

Figure S23. UV-vis spectra of (a) $\mathbf{1}^{P}$, (b) $\mathbf{3}^{O}$ and (c) $\mathbf{4}^{O}$ in MeTHF at –130 ºC.

10. Resonance Raman (rR) data

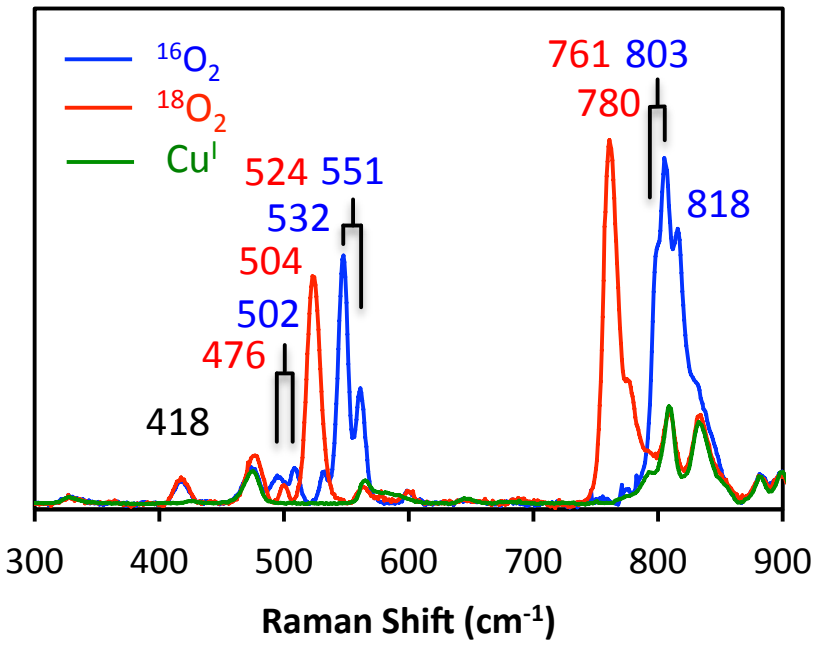

Figure S24. Resonance Raman spectra of $\mathbf{1^P}$ with 647 nm excitation. While the $^{16}O_2$ spectrum contains a number of additional vibrations, the number of vibrations in the $^{18}O_2$ spectrum is consistent with a mixture of *syn* and *anti* ^{DMM}ESE; two ν_{O-O} (780 and 761 cm^{-1}) and three ν_{Cu-O} (the symmetric Cu–O stretch at 524 and 504 cm^{-1} and the asymmetric Cu–O stretch at 476 cm^{-1}). From group theory considerations, the asymmetric ν_{Cu-O} is forbidden in the anti isomer and allowed from the *syn* isomer due to the lower symmetry of its Cu_2O_2 core, see reference ** for details. If we assume that $\mathbf{1^P}$ only contains the *syn* and *anti* isomers, the additional vibrations observed in the $^{16}O_2$ spectrum could arise from a Fermi resonance with an un-observed vibration. With this assumption, we favor an assignment of two ν_{O-O} at 818 cm^{-1} and an 803 cm^{-1} (spit into two vibrations at 799 and 806 cm^{-1}), one symmetric ν_{Cu-O} at at 551 cm^{-1} (split into 561 and 547 cm^{-1}), another symmetric ν_{Cu-O} at 532 cm^{-1}, and an asymmetric ν_{Cu-O} at 502 cm^{-1} (split into 508 and 495 cm^{-1}). These assignments are consistent with the appropriate intensities, energies, and isotope shifts of each band relative to the $^{18}O_2$ spectrum and those of previously characterized end-on peroxo complexes. However, the presence of an additional molecular species cannot be ruled out. Additionally, the isotope insensitive $Cu–N_{amine}$ vibration is observed at 418 cm^{-1}.

** "Observation of a $Cu(II)_2(\mu$-1,2-peroxo$)/Cu(III)_2(\mu$-oxo$)_2$ Equilibrium and its Implications for Copper-Dioxygen Reactivity" Kieber-Emmons, M. T.; Ginsbach, J. W.; Wick, P. K.; Lucas, H. R.; Helton, M. E.; Lucchese, B.; Suzuki, M.; D., Z. A.; Karlin, K. D.; Solomon, E. I. *Angew Chem., Int. Ed.* **2014**, 53, 4935-4939.

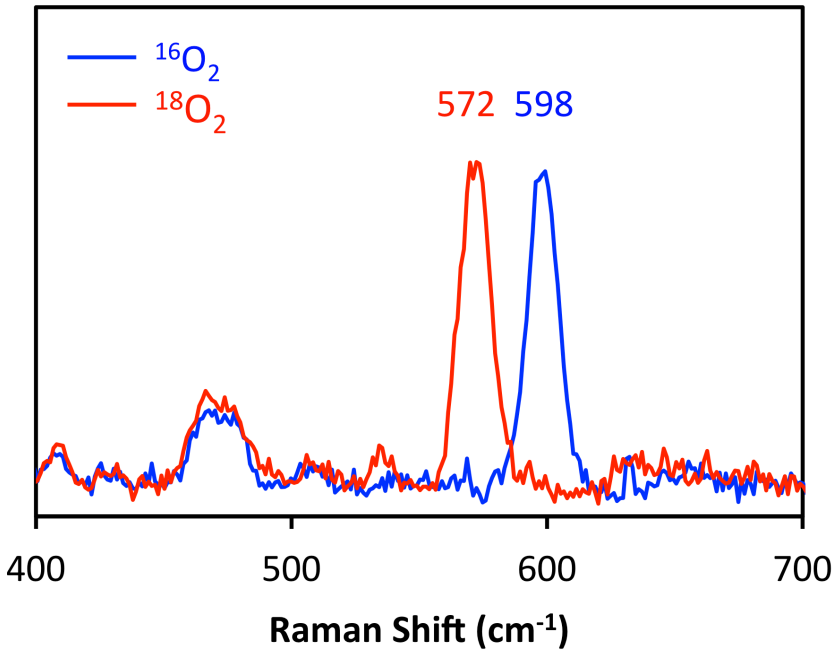

Figure S25. Resonance Raman spectra of $\mathbf{2}^{\mathbf{O}}$-($CH_3SO_3^-$) with 380 nm excitation in MeTHF collected at 77 K. See text.

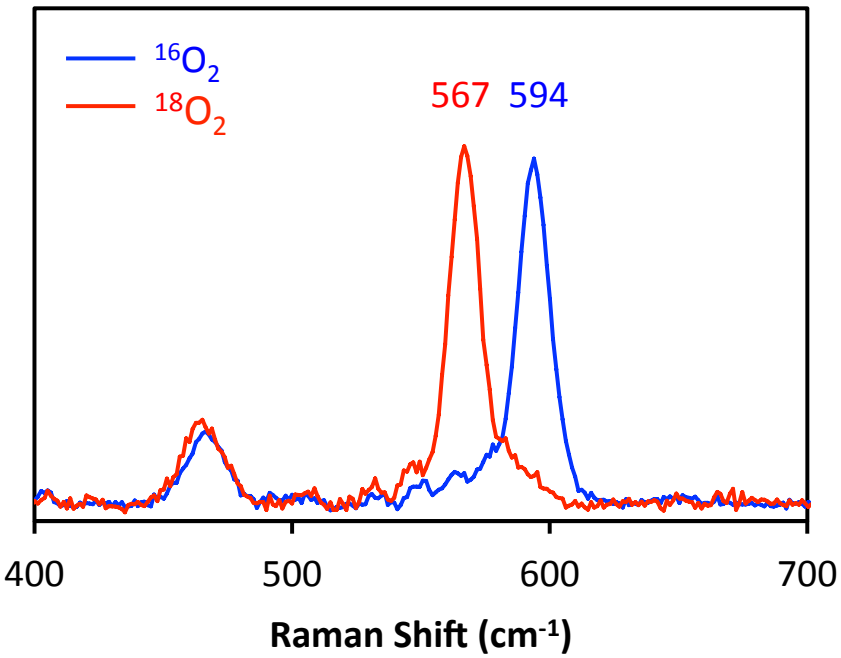

Figure S26. Resonance Raman spectra of $\mathbf{3}^{\mathbf{O}}$ with 380 nm excitation in MeTHF collected at 77 K. See text.

11. Reactivity Study

A Schlenk cuvette was charged with 2.5 mL of a 0.25 mM solution of $[(^{DMM}ESP)Cu^{I}][B(C_6F_5)_4]$ in MeTHF. The cuvette was sealed with a septum and secured with a plastic zip tie. This cell was transferred to the pre-cooled cryostat and allowed to chill at –130 °C with a minimum of 10 minutes allowed for equilibration prior to oxygenation. Oxygenation of the copper samples was achieved by slowly bubbling dioxygen through the solution with a Hamilton gastight syringe to generate a trans-peroxo species ($\mathbf{2^P}$). After addition of dioxygen, 1 equiv of tetrabutylammonium methanesulfonate ($CH_3SO_3^-$) was added to form a pure bis-μ-oxo species ($\mathbf{2^O}$). After the full formation of $\mathbf{2^O}$, 100 μL of stock solution of PPh_3 (2.5 mM) was added to $\mathbf{2^O}$. It slowly reacted with PPh_3 over 3 ~ 4 hours. After the reaction, all solvent was removed by a reduced vacuum and then dissolved in 5 mL acetone. The ESI-MS of the acetone was recorded exhibiting an intense PPh_3=O peak and no ligand sulfoxidation observed. Under identical condition, when an excess of PPh_3 was added to the $\mathbf{2^P}$ and $\mathbf{2^O}$ mixture, both species were slowly decomposed for 2 ~ 3 hours. After low temperature workup, it showed that no ligand sulfoxidation occurred but PPh_3=O formed.

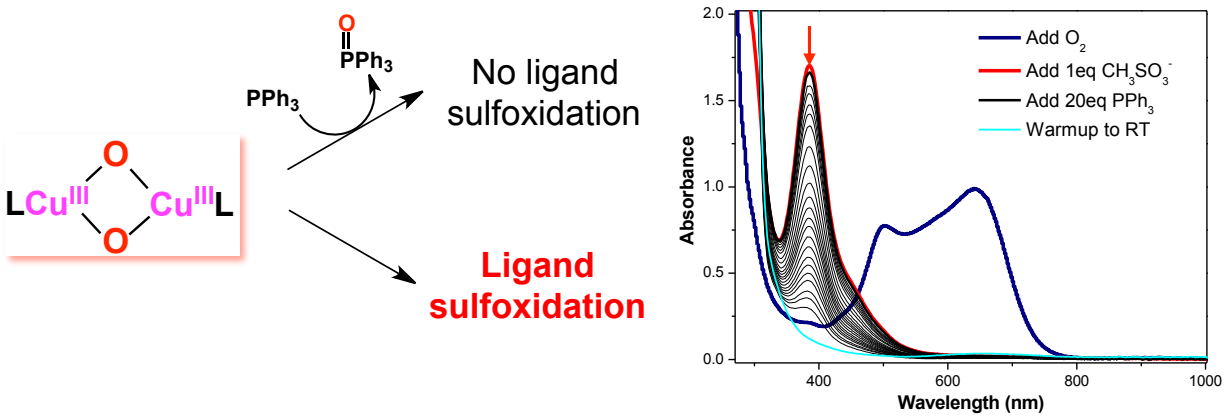

Figure S27. The reaction of $\mathbf{2^O}$ with 20 eq PPh_3 in MeTHF at –130 °C for 3 ~ 4 hours.

12. Ligand sulfoxidation

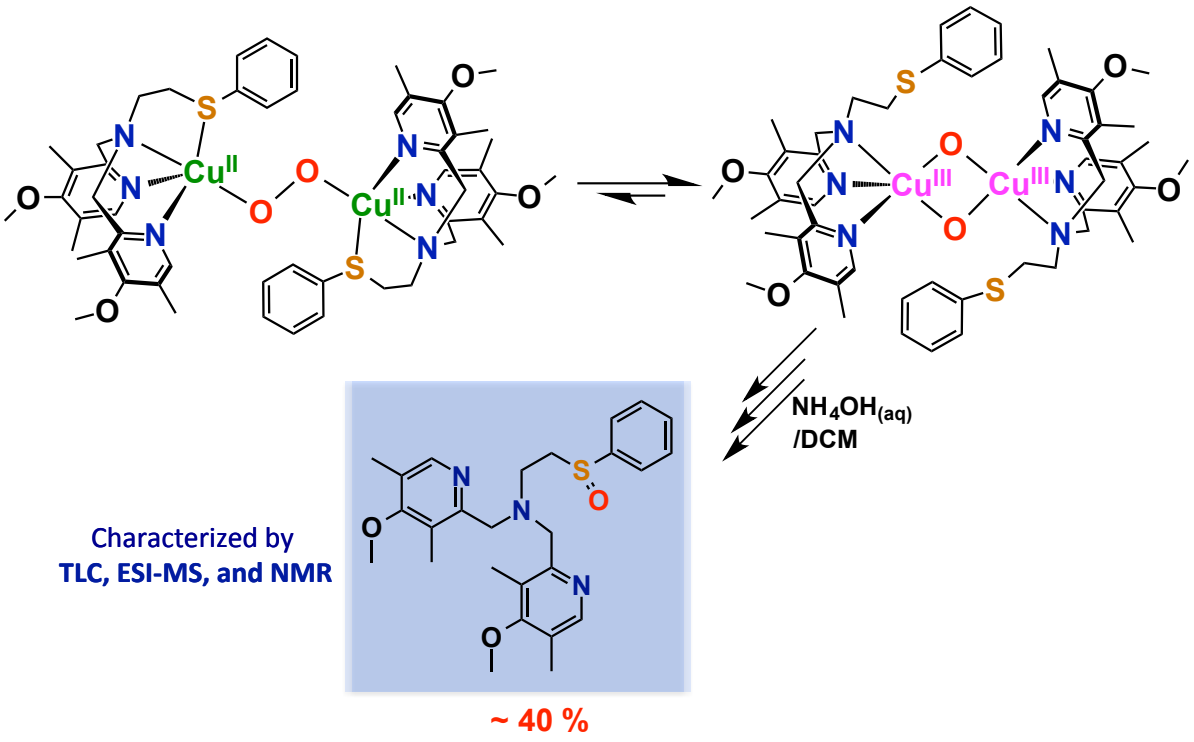

(a) Sulfoxidation of ^{DMM}ESP in 2^{O}. [(^{DMM}ESP)Cu^{I}]B(C_6F_5)$_4$ **(2)**, (684 mg, 0.5728 mmol) was dissolved in 30 mL of MeTHF and the pale yellow solution was cooled to –120 ~ –125 ^{o}C by the use of an Pentane/N_2(*l*) bath. Upon oxygenation, an intense indigo trans-peroxo species, $\mathbf{2^{P}}$ was generated and isomerized to a bis-μ-oxo species $\mathbf{2^{O}}$. Both species were kept at –120 ~ –125 ^{o}C and were stirred for 6 ~ 7 hours showing color change from blue to green. All solvent was removed by reduced vacuum at low temperature. The residual material was treated with 100 mL of saturated Na_2EDTA/H_2O solution, and the organic part was extracted by using 50 mL of CH_2Cl_2 three times. The organic fractions were combined, dried over anhydrous $MgSO_4$, filtered, and concentrated by the reduced vacuum, yielding crude dark yellow oil. The isolation and purification by column chromatography (Al_2O_3, 100 % ethyl acetate) revealed unreacted ligand ^{DMM}ESP (R_f = 0.82, ~ 40% yield) and the sulfoxide product (R_f = 0.45, ~ 40% yield). Products were characterized by ESI-MS and ^{1}H-NMR.

Sulfoxide product of ^{DMM}ESP: **^{1}H-NMR** (400 MHz, $CDCl_3$): δ 8.13 (s, 2H), 7.42-7.35 (m, 5H), 3.85-3.82 (d, 2H of N-CH_2-Py), 3.76-3.72 (d, 2H of N-CH_2Py), 3.71 (s, 6H), 3.05-3.03 (t, 2H), 2.83-2.79 (t, 2H), 2.23 (s, 6H), 2.16 (s, 6H) (**Figure S28**). **ESI-MS**, *m*/*z*: 467.73 in acetone at room temperature (**Figure S30**).

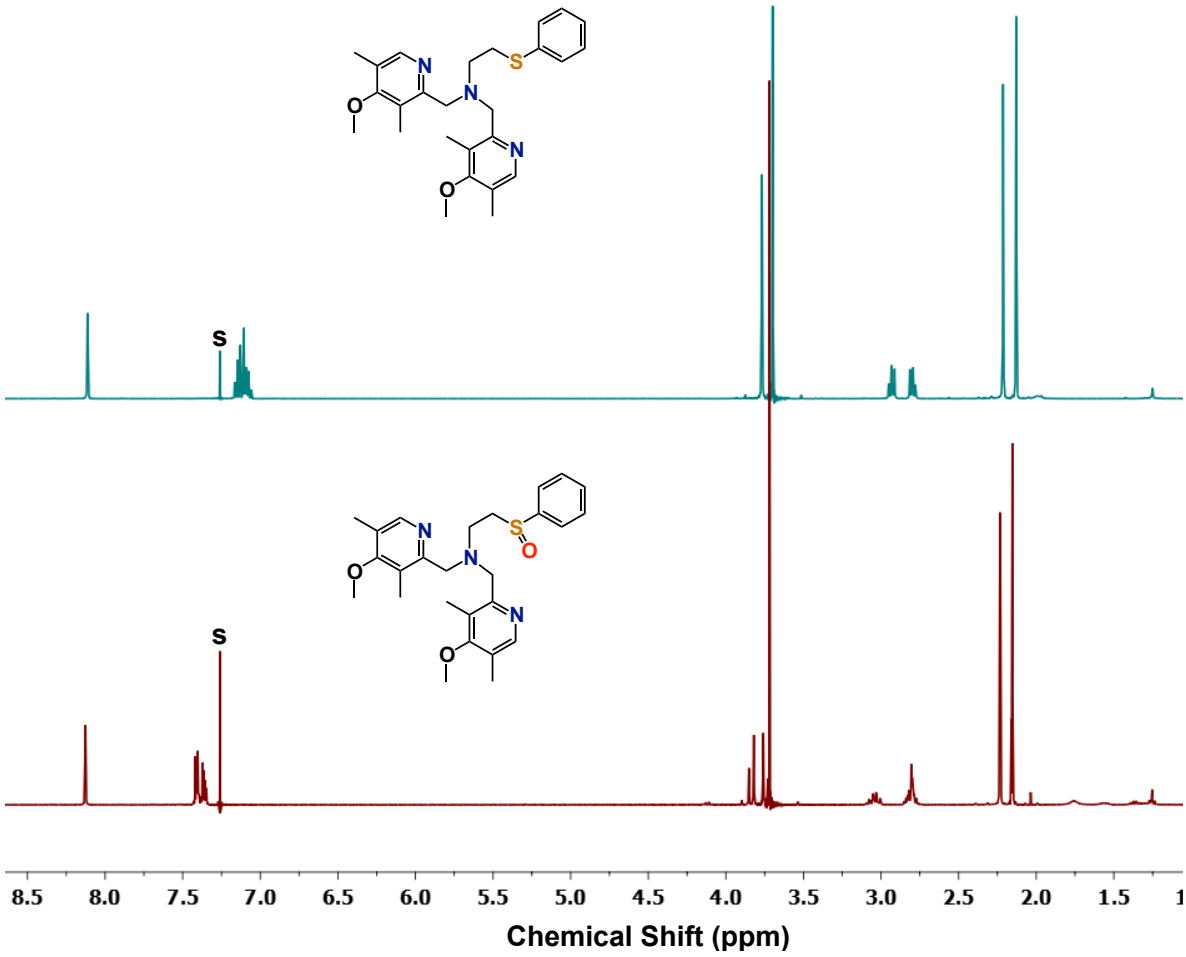

Figure S28. ^{1}H-NMR (400 MHz, $CDCl_3$) data of ^{DMM}ESP ligand and sulfoxide product of ^{DMM}ESP (s denotes peaks due to residual hydrogen atoms in the solvent).

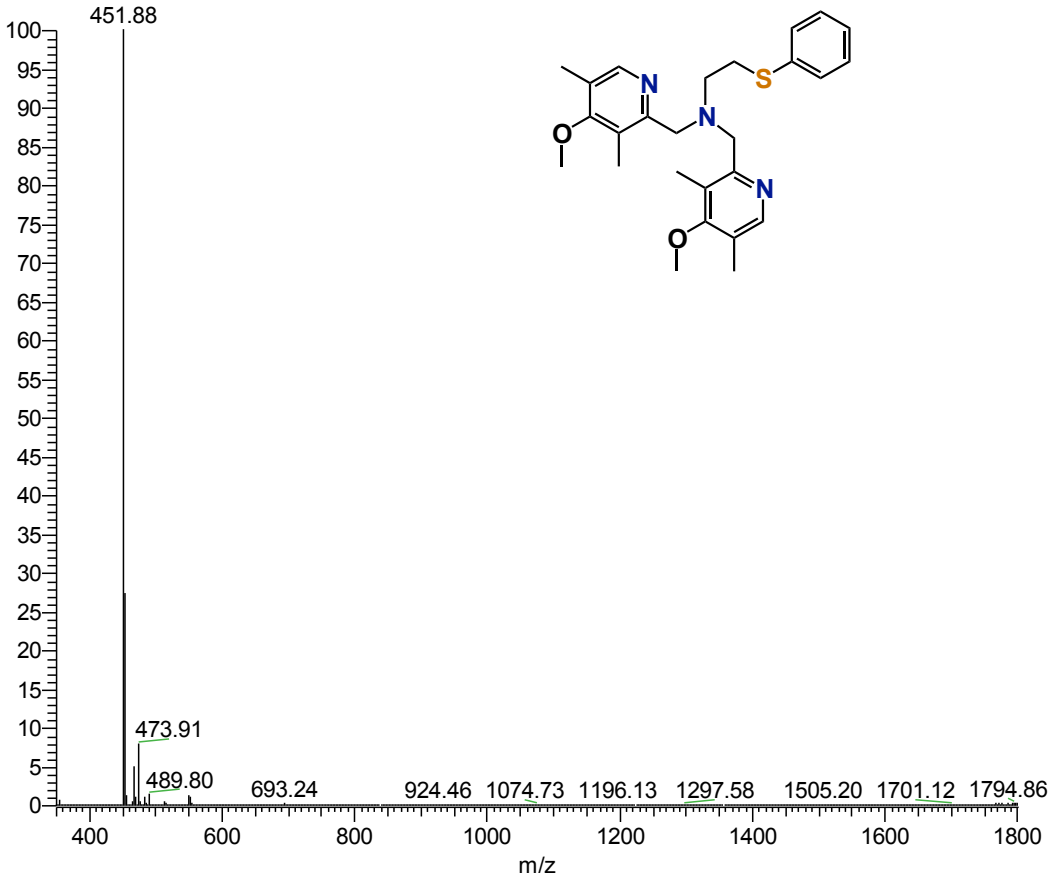

Figure S29. ESI-MS of ^{DMM}ESP ligand (*m*/*z*: 451.88) in acetone at room temperature.

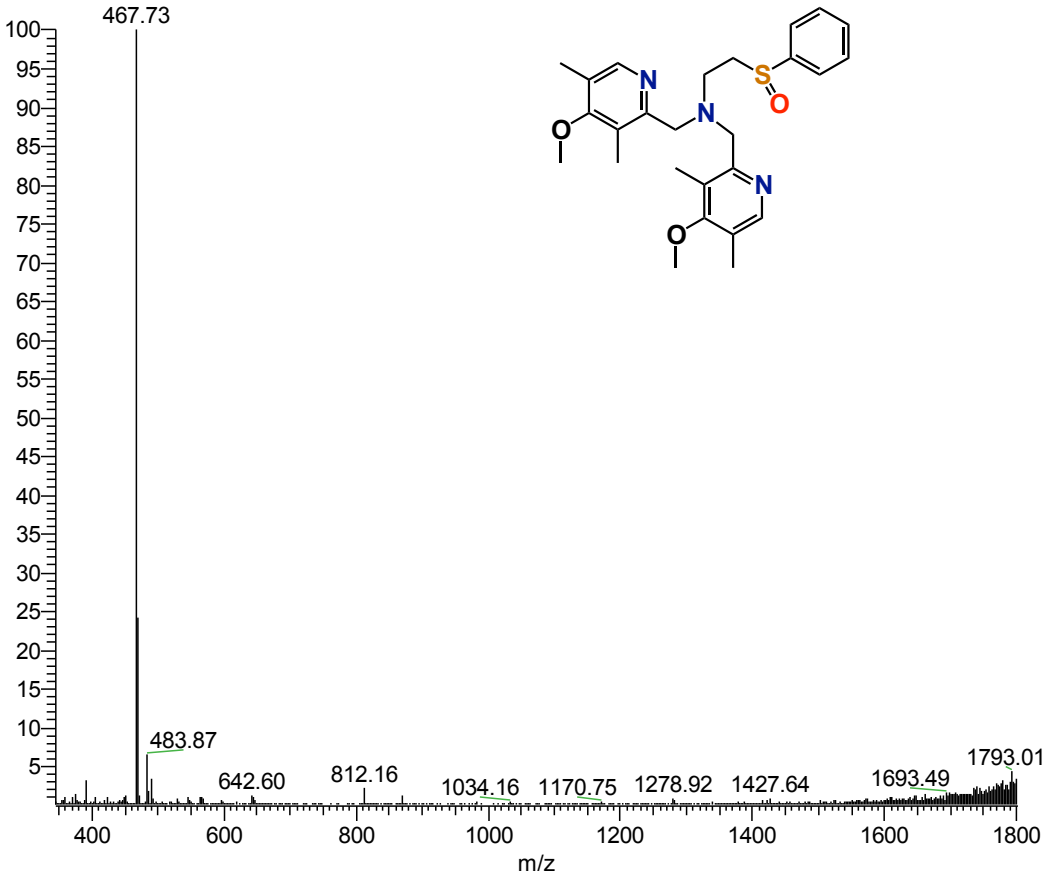

Figure S30. ESI-MS of the sulfoxide product of ^{DMM}ESP ligand (*m*/*z*: 467.73) in acetone at room temperature.

(b) Sulfoxidation of ^{DMM}ESDP in 3^{O}. Following a similar methodology as described above in Section 10(a), the same behavior was also observed for **3^{O}** resulting in the 43 % sulfoxide product (R_f = 0.26 over Al_2O_3 with 100 % ethyl acetate).

^{DMM}ESDP ligand: (Alumina, 100 % ethylacetate, R_f = 0.67) **^{1}H-NMR** (400 MHz, $CDCl_3$): δ 8.11 (s, 2H), 6.93-6.81(m, 3H), 3.77 (s, 4H), 3.70 (s, 6H), 2.89-2.86 (t, 2H), 2.79-2.75 (t, 2H), 2.25-2.13 (s, 12H), 2.13 (s, 6H). **ESI-MS**, *m*/*z*: 480.50 ($M + H^+$).

Sulfoxide product of ^{DMM}ESDP: **^{1}H-NMR** (400 MHz, $CDCl_3$): δ 8.16 (s, 2H), 7.61-7.59 (d, 1H), 7.12-7.09 (d, 1H), 6.92 (s, 1H), 3.72 (s, 4H), 3.67 (s, 6H), 3.10-2.65 (m, 4H of N-CH_2-CH_2-S-), 2.29 (s, 3H), 2.19 (s, 3H), 2.16 (s, 6H), 2.08 (s, 6H) (**Figure S31**). **ESI-MS**, *m*/*z*: 495.79 in acetone at room temperature (**Figure S33**).

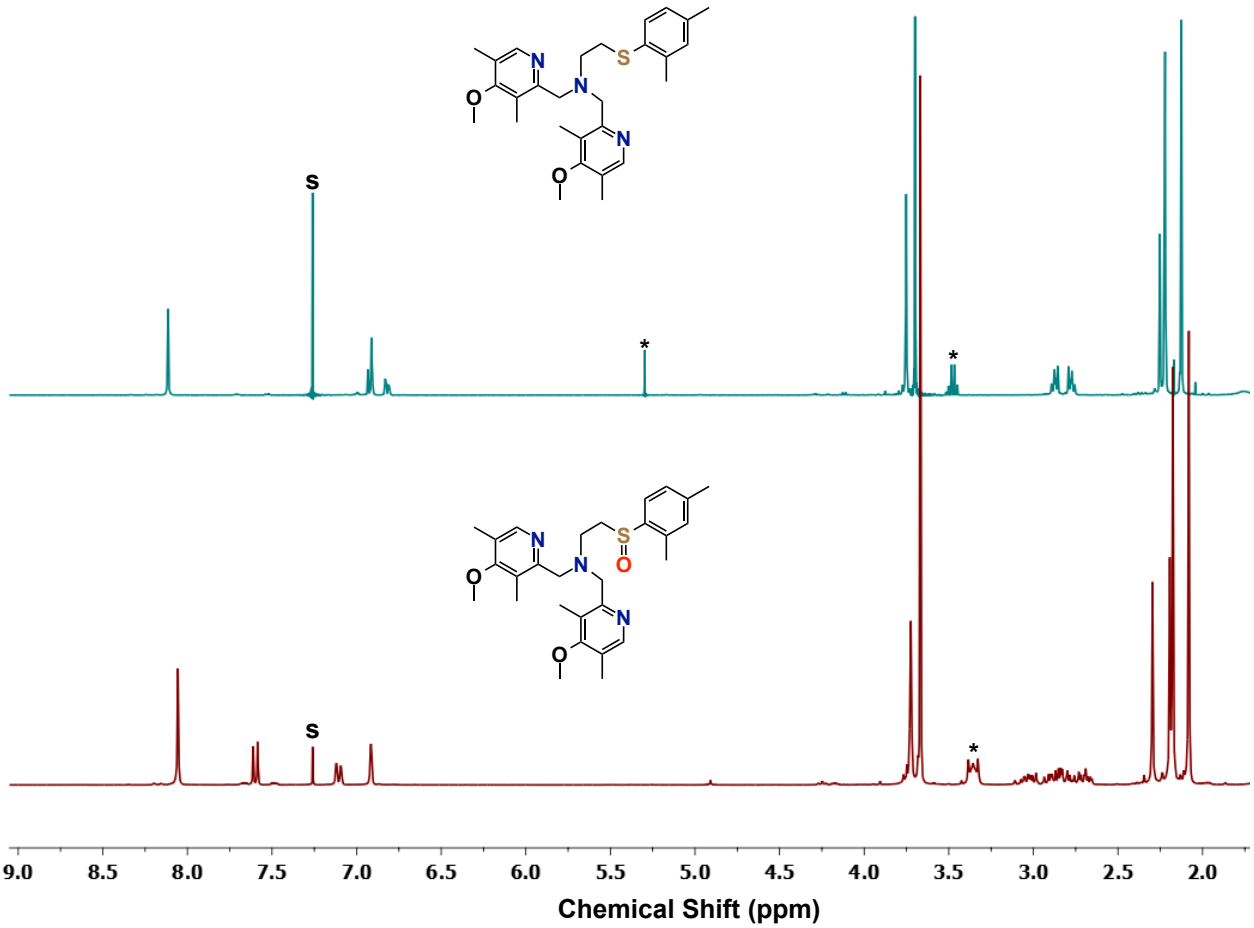

Figure S31. ^{1}H-NMR (400 MHz, $CDCl_3$) data of ^{DMM}ESDP ligand and sulfoxide product of ^{DMM}ESDP ("s" denotes peaks due to residual hydrogen atoms in the solvent; *indicates traces of solvents in the products).

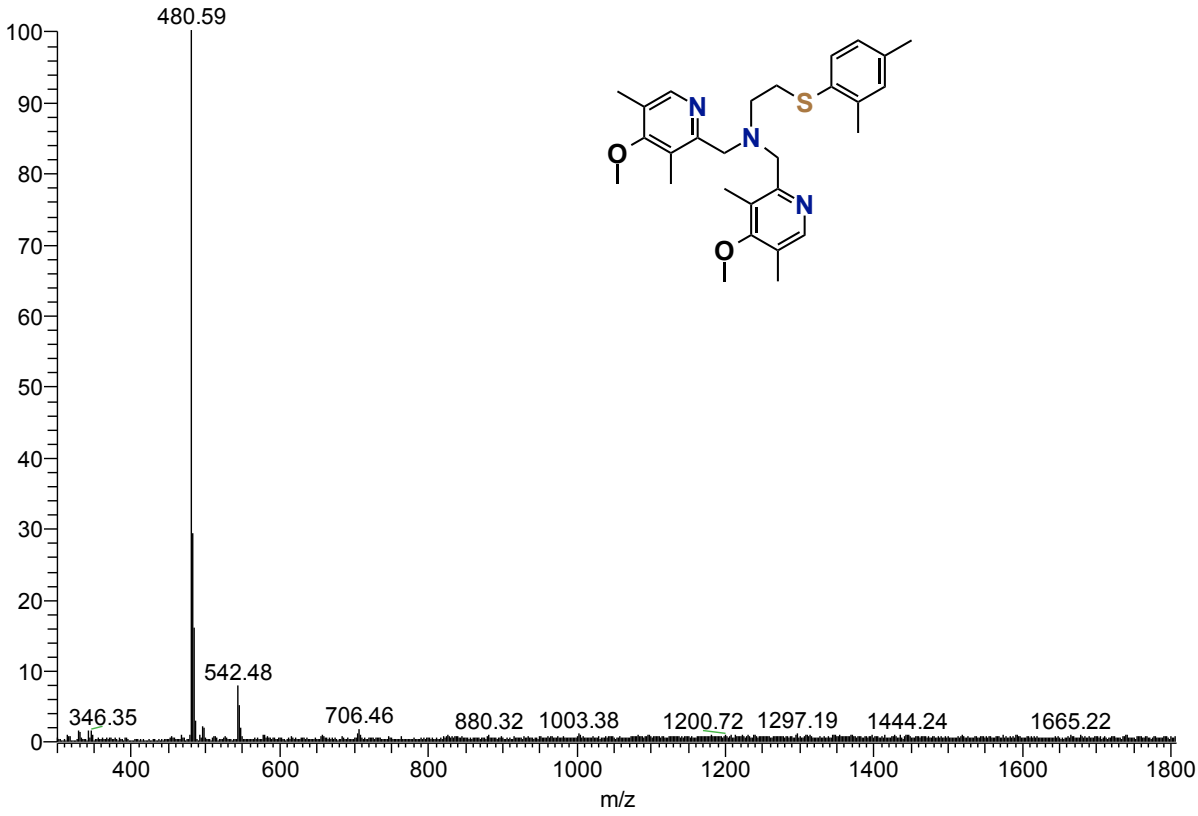

Figure S32. ESI-MS of ^{DMM}ESDP ligand (*m*/*z*: 480.59) in acetone at room temperature.

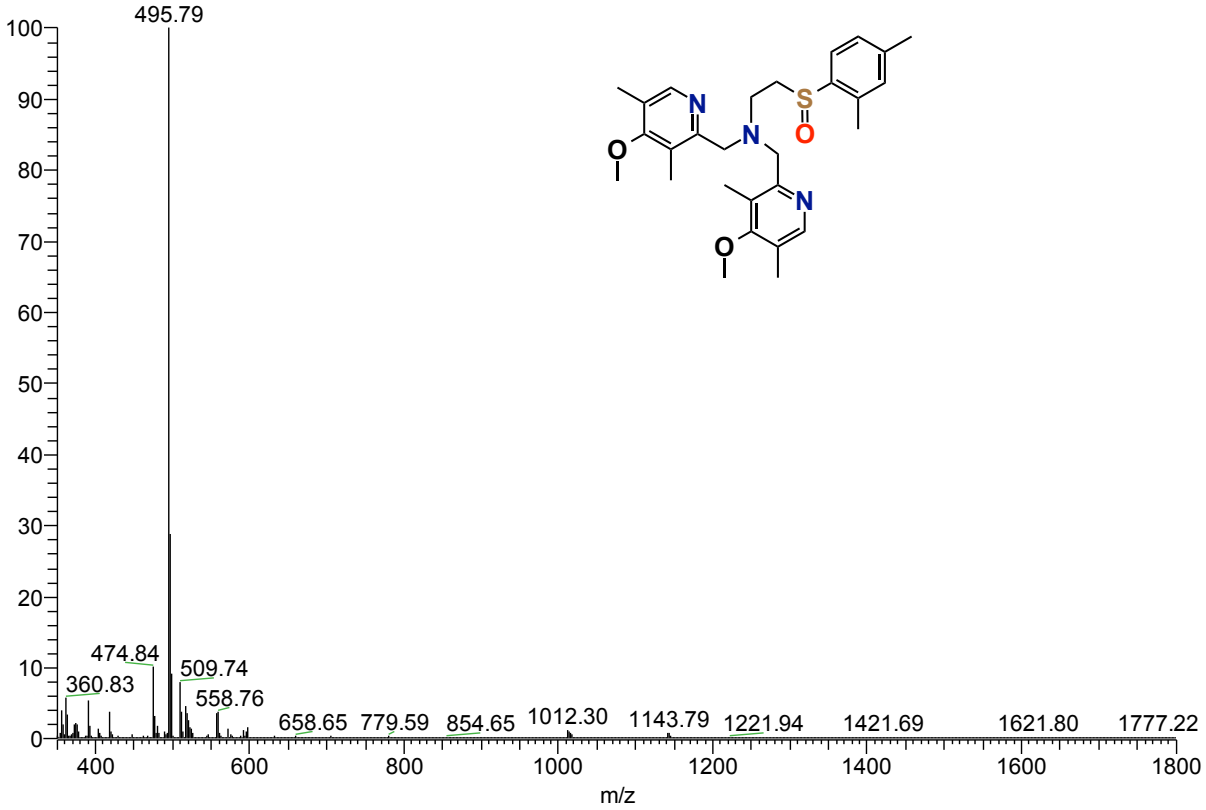

Figure S33. ESI-MS of the sulfoxide product of ^{DMM}ESDP ligand (*m/z*: 495.79) in acetone at room temperature.

Table S3. UV-vis and resonance Raman spectroscopic data for copper–dioxygen adducts.

Complex	LMCT; λ_{max} nm (ε, M^{-1} cm^{-1})	Solvent Temp	$\nu_{O\text{-}O}$; $\Delta(^{18}O_2)$;cm^{-1}	$\nu_{Cu\text{-}O}$; $\Delta(^{18}O_2)$;cm^{-1}
$[\{(TMPA)Cu^{II}\}_2(\mu\text{-}1,2\text{-}O_2^{2-})]^{2+}$	435 (1,700) 524 (11,300) 615 (5,800) [a]	EtCN –80	832; –44	561; –26
$[\{(ESE)Cu^{II}\}_2(\mu\text{-}1,2\text{-}O_2^{2-})]^{2+}$	445 (2,600) 530 (9,200) 605 (11,800) [b]	MeTHF –128	817; –46	545; –26
$[\{(^{DMM}ESE)Cu^{II}\}_2(\mu\text{-}1,2\text{-}O_2^{2-})]^{2+}$ (**1^{P}**)	445 (2,150) 521(8,640) 615 (10,850) [c]	MeTHF –130	818/803; -38/-42	551/532; -27/-28
$[\{(^{DMM}ESP)Cu^{II}\}_2(\mu\text{-}1,2\text{-}O_2^{2-})]^{2+}$ (**2^{P}**)	504 644 [c]	MeTHF –130	830/810; -46/-38	545/531; -27/-31
$[\{(^{DMM}ESP)Cu^{III}\}_2(\mu\text{-}O^{2-})_2]^{2+}$ (**2^{O}**)	388 [c]	MeTHF –130		597; -27
$[\{(^{DMM}ESP)Cu^{III}\}_2(\mu\text{-}O^{2-})_2]^{2+}$ **(2^{O}-CH$_3$SO$_3^-$)**	386 (13,000) [c]	MeTHF –130		598; -26
$[\{(^{DMM}ESDP)Cu^{III}\}_2(\mu\text{-}O^{2-})_2]^{2+}$ (**3^{O}**)	388 (13,000) [c]	MeTHF –130		594; -27
$[\{(^{DMM}EOE)Cu^{III}\}_2(\mu\text{-}O^{2-})_2]^{2+}$ (**4^{O}**)	382 (20,500)[c]	MeTHF –130		–

[a] ref 12,13, [b] ref 14 and [c] this work.

13. References

(1) Hatcher, L. Q.; Lee, D.-H.; Vance, M. A.; Milligan, A. E.; Sarangi, R.; Hodgson, K. O.; Hedman, B.; Solomon, E. I.; Karlin, K. D. *Inorg. Chem.* **2006,** *45*, 10055-10057.

(2) Tyeklár, Z.; Jacobson, R. R.; Wei, N.; Murthy, N. N.; Zubieta, J.; Karlin, K. D. *J. Am. Chem. Soc.* **1993,** *115*, 2677-2689.

(3) Zhang, C. X.; Kaderli, S.; Costas, M.; Kim, E.-i.; Neuhold, Y.-M.; Karlin, K. D.; Zuberbühler, A. D. *Inorg. Chem.* **2003,** *42*, 1807-1824.

(4) Maiti, D.; Woertink, J. S.; Vance, M. A.; Milligan, A. E.; Narducci Sarjeant, A. A.; Solomon, E. I.; Karlin, K. D. *J. Am. Chem. Soc.* **2007,** *129*, 8882-8892.

(5) Fry, H. C.; Lucas, H. R.; Narducci Sarjeant, A. A.; Karlin, K. D.; Meyer, G. J. *Inorg. Chem.* **2008,** *47*, 241-256.

(6) Canary, J. W.; Mortezaei, S.; Liang, J. *Chem. Commun.* **2010,** *46*, 5850-5860.

(7) Kretzer, R. M.; Ghiladi, R. A.; Lebeau, E. L.; Liang, H.-C.; Karlin, K. D. *Inorg. Chem.* **2003,** *42*, 3016-3025.

(8) Lee, D.-H.; Hatcher, L. Q.; Vance, M. A.; Sarangi, R.; Milligan, A. E.; Narducci Sarjeant, A. A.; Incarvito, C. D.; Rheingold, A. L.; Hodgson, K. O.; Hedman, B.; Solomon, E. I.; Karlin, K. D. *Inorg. Chem.* **2007,** *46*, 6056-6068.

(9) Lee, Y.; Lee, D.-H.; Park, G. Y.; Lucas, H. R.; Narducci Sarjeant, A. A.; Kieber-Emmons, M. T.; Vance, M. A.; Milligan, A. E.; Solomon, E. I.; Karlin, K. D. *Inorg. Chem.* **2010,** *49*, 8873-8885.

(10) Jaron, S.; Blackburn, N. J. *Biochemistry* **1999,** *38*, 15086-15096.

(11) Blackburn, N. J.; Pettingill, T. M.; Seagraves, K. S.; Shigeta, R. T. *J. Biol. Chem.* **1990,** *265*, 15383-15386.

(12) Jacobson, R. R.; Tyeklar, Z.; Farooq, A.; Karlin, K. D.; Liu, S.; Zubieta, J. *J. Am. Chem. Soc.* **1988,** *110*, 3690-3692.

(13) Baldwin, M. J.; Ross, P. K.; Pate, J. E.; Tyeklar, Z.; Karlin, K. D.; Solomon, E. I. *J. Am. Chem. Soc.* **1991,** *113*, 8671-8679.

(14) Lee, D.-H.; Hatcher, L. Q.; Vance, M. A.; Sarangi, R.; Milligan, A. E.; Narducci Sarjeant, A. A.; Incarvito, C. D.; Rheingold, A. L.; Hodgson, K. O.; Hedman, B.; Solomon, E. I.; Karlin, K. D. *Inorg. Chem.* **2007,** *46*, 6056-6068.